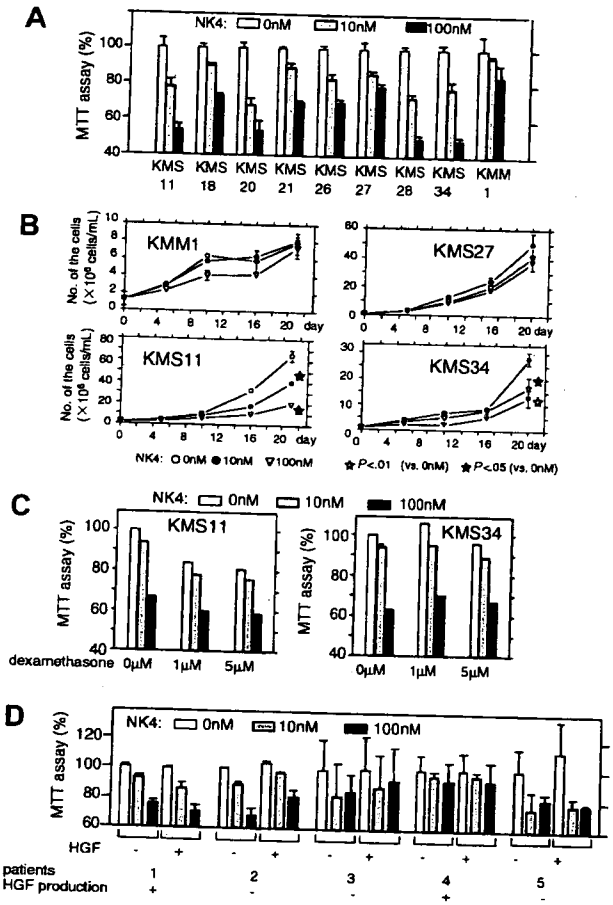

Figure 2. In vitro growth inhibition of MM cells by NK4 protein. (A) MM cell lines (2×10^5 cells/mL) were cultured for 48 hours with the indicated concentrations of NK4 protein in RPMI containing 4% dialyzed FCS. Proliferation was evaluated by MTT assay. (B) Cells (2×10^5/mL) were cultured with the indicated concentrations of NK4 protein in RPMI containing 10% FCS. The number of cells was adjusted to 2×10^5/mL every passage. The number of live cells was counted every 5 days using the trypan blue exclusion test. (C) Antimyeloma effects of NK4 protein in combination with Dex treatment. NK4 protein was added to the culture medium in the presence of Dex. KMS11 is a Dex-sensitive MM line, and KMS34 is a Dex-resistant line. Proliferation was evaluated by MTT assay as described. (D) Primary MM cells obtained from the patients were cultured for 48 hours with various concentrations of NK4 or HGF (or both) in RPMI containing 4% dialyzed FCS, and an MTT assay was conducted. For all studies in panels A-D, the mean ± one SD, each in triplicate, is shown.

Growth inhibition and induction of apoptosis of MM cells in vitro

The in vitro proliferation of MM cells in the presence or absence of NK4 protein was examined (Figure 2A-B). In the MTT assay conducted in RPMI containing 4% dialyzed FCS, NK4 was found to inhibit the proliferation of HGF-producing KMS11 and KMS34 cells and also induced inhibition of the growth of cells not producing HGF (Figure 2A). The reason for growth suppression in non–HGF-producing cells was most likely due to an additional yet still unknown function of NK4 rather than the antagonistic inhibition of HGF, which is addressed in detail in "Discussion." The time-course changes in cell number in the presence and absence of NK4 were also examined in RPMI containing 10% FCS (Hyclone Laboratories; Figure 2B). NK4 was thus found to regulate growth of KMS11 and KMS34 cells.

Because glucocorticoid is a key drug used for the treatment of MM, combination treatment with NK4 together with Dex was also examined by MTT assay (Figure 2C). KMS11 is a Dex-sensitive cell line, and NK4 enhanced Dex-induced growth inhibition of KMS11 cells in a dose-dependent manner. NK4 also regulated the proliferation of Dex-resistant KMS34 cells in a manner that was also dependent on the concentration of NK4.

NK4-induced growth inhibition of primary MM cells was also examined by MTT assay. As shown in Figure 2D, NK4 also inhibited the proliferation of primary bone marrow MM cells significantly in patients 1, 2, and 5 and weakly in patients 3 and 4 regardless of HGF production.

Induction of apoptosis by NK4 was also quantified by flow cytometry using annexin V and propidium iodide staining in KMS27 and KMS34 cells (Figure 3). NK4 treatment increased the annexin V^+ fraction in both cell lines. Neutralizing anti-HGF antibody also induced apoptosis in non–HGF-producing KMS27 cells, probably because the antibody reacted with a very small amount of HGF present as a contaminant in FCS (Hyclone Laboratories). Addition of an excess amount of HGF blocked neutralizing antibody-induced apoptosis, whereas addition of exogenous HGF only partially inhibited NK4-induced apoptosis in KMS27 cells. Culture with both NK4 and neutralizing antibody revealed a further increase in the annexin V fraction in KMS27 and

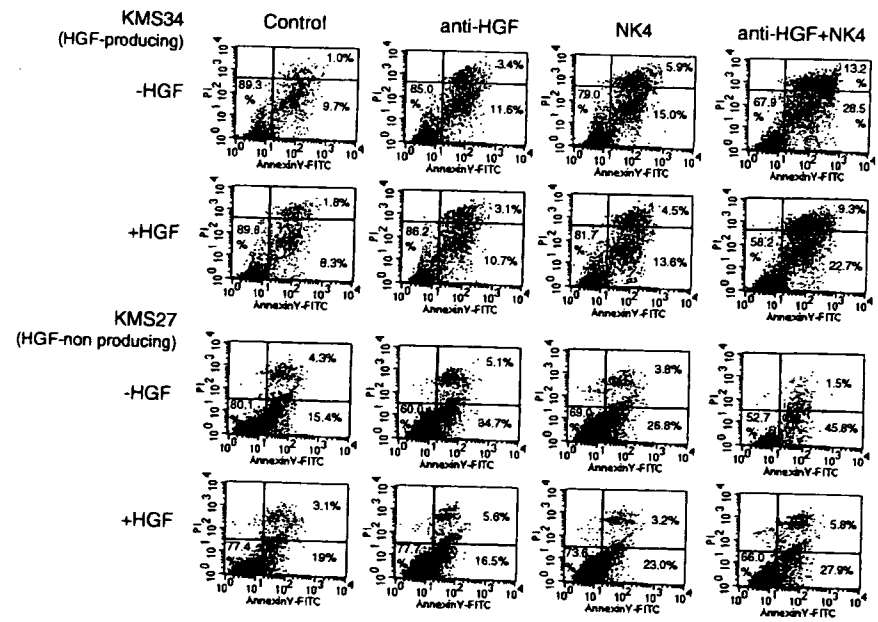

Figure 3. Flow cytometric analysis for quantification of apoptotic cells. MM cells (2×10^5/mL were cultured in RPMI containing 10% FCS (Hyclone Laboratories) and collected after 4 days of exposure to NK4 (100 nM) or anti–HGF-neutralizing monoclonal antibody (19 μg/mL) in the presence or absence of 100 ng/mL HGF; this concentration of HGF was an excess amount sufficient to counteract NK4 or the neutralizing antibody. Cells were stained with FITC-coupled annexin V and propidium iodide. Induction of apoptosis by NK4 was evaluated by flow cytometry. The percentages of early apoptotic cells (annexin V^+/PI^-) and late apoptotic cells (annexin V^+/PI^+) are indicated in the corresponding quadrants.

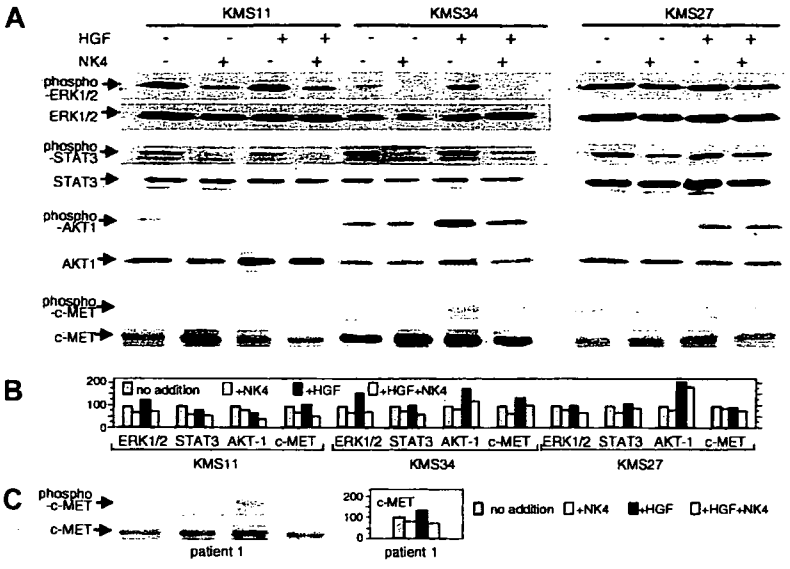

Figure 4. Western blot analysis of activated ERK1/2, STAT3, and AKT-1, and immunoprecipitation and Western blot analysis of activated c-MET in NK4-treated MM cells. (A) HGF-producing KMS11 and KMS34 cells as well as non–HGF-producing KMS27 cells were treated with 200 nM NK4 protein in RPMI containing 4% dialyzed FCS overnight; the cells were then incubated with or without 50 ng/mL HGF at room temperature for 20 minutes. The cell lysates were subjected to sodium dodecyl sulfate-polyacrylamide gel electrophoresis (SDS-PAGE), followed by immunoblotting with anti–phospho-ERK1/2, anti–phospho-STAT3, and anti–phospho-Ser473 AKT-1 antibodies. Blots were stripped and reprobed with anti-ERK1/2, anti-STAT3, and anti–AKT-1 antibodies. For evaluation of c-MET activation, MM cell lines were also treated with 200 nM NK4 in RPMI containing 4% dialyzed FCS overnight, and then incubated with or without 50 ng/mL HGF at room temperature for 5 minutes. After immunoprecipitation with anti–c-MET antibody, the immunocomplexes were subjected to SDS-PAGE. Immunoblotting was conducted with anti–phospho–c-MET antibody, and then the same filters were stripped and reprobed with anti–c-MET. (B) Densitometric analysis of the activation of c-MET and signal transducers. (C) Evaluation of c-MET activation in primary MM cells obtained from patient 1. Treatment of the MM cells and immunoprecipitation followed by Western blot analysis were performed as described.

KMS34 cells. These results suggested that not only the antagonistic inhibition of HGF but also the additional, unknown effects of NK4 mentioned are important for induction of apoptosis in MM cells.

NK4 regulation of the activation of ERK1/2, STAT3, AKT-1, and c-MET in MM cells

To examine the effects of NK4 on intracellular signaling, the phosphorylation status of ERK1/2, STAT3, and AKT-1 was examined by Western blot analysis, because these 3 signal transducers are key molecules in the growth of MM cells. As shown in Figure 4, baseline as well as HGF-induced phosphorylation of ERK1/2, STAT3, and AKT-1 was inhibited by NK4 treatment in HGF-producing KMS11 and KMS34 cell lines. Immunoprecipitation using anti–c-MET antibody and Western blot analysis using anti–phosphorylated c-MET antibody revealed that phosphorylation of c-MET was also inhibited by NK4 in these cells. The results suggested that in HGF-producing cells ERK1/2, STAT3, and AKT-1 are phosphorylated to different extents through autocrine activation of the c-MET and that NK4 inhibits phosphorylation of these signaling molecules by antagonizing functional association between HGF and c-MET. KMS11 cells showed lower responsiveness to exogenous HGF compared with KMS34 cells probably because KMS11 cells produced much higher amount of HGF by themselves than other cells as shown in Figure 1. Densitometric analysis showed that the phosphorylation of these 3 signal transducers and c-MET was also inhibited weakly by NK4 treatment in non–HGF-producing KMS27 cells. Baseline phosphorylation in the absence of HGF is relatively high in this cell line. Consequently, the phosphorylation level of c-MET was not significantly changed by addition of NK4 or exogenous HGF (Figure 4). Immunoprecipitation and Western blot analysis revealed that NK4 protein inhibited phosphorylation of c-MET in the primary MM cells obtained from patient 1 (Figure 4C).

Growth inhibition of MM cells in vivo by adenovirus-mediated gene transfer of NK4

To examine the antimyeloma effects of NK4 in vivo, the NK4 gene was transduced to tumor-bearing Icr/scid mice using the recombinant adenovirus. Because MM is a systemic disease, the systemic delivery of NK4 protein is necessary. Thus, instead of intratumoral injection, we chose to apply intramuscular injection at the femur. To confirm that the adenoviral vector indeed expressed the NK4 protein, an immunoblot analysis was initially performed, and 67 kDa of the NK4 protein was identified in the culture medium of the NK4-infected cells (Figure 5A). The next question to be addressed

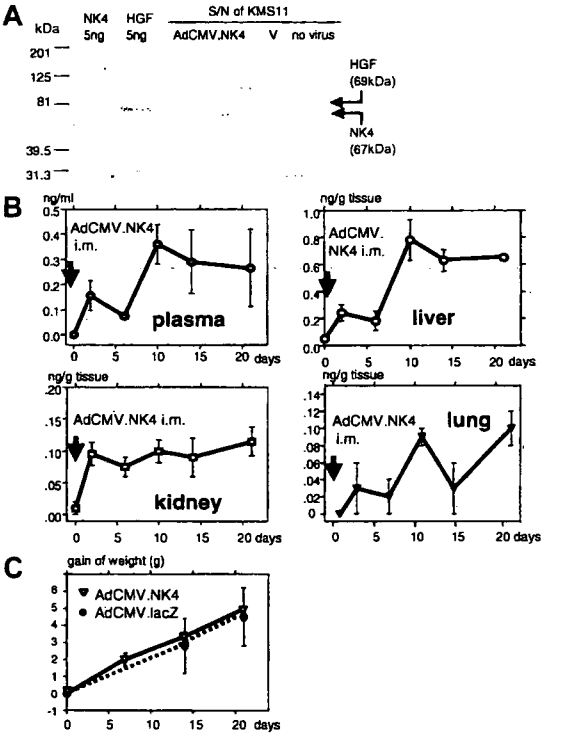

Figure 5. Production of the NK4 gene product by the AdCMV.NK4 vector and intramuscular injection of AdCMV.NK4 in Icr/scid mice. (A) AdCMV.NK4 was used to infect KMS 11 cells at multiplicity of infection (MOI) 30. Supernatant (5 μL) was subjected to Western blot analysis. Rabbit anti-HGF polyclonal antibody enabled the detection of a 67-kDa NK4 gene product. (B) Pharmacokinetic study of the NK4 gene product. Infectious particles (5×10^8/mL) of AdCMV.NK4 were injected into the femoral muscle of 5-week-old male Icr/scid mice on day 0 (arrow). On days 0, 3, 7, 10, 14, and 21, 3 mice were killed. Tissue lysates were obtained by immersing various organs in the lysis buffer overnight. The concentrations of NK4 in the plasma and tissue lysates were examined by ELISA. (C) Change in the weight of AdCMV.NK4-treated mice. A total of 5×10^8 infectious particles/mL AdCMV.NK4 or AdCMV.lacZ were injected into the femoral muscle of 5-week-old male Icr/scid mice. Changes in weight are shown. Each group consists of 3 mice.

was whether the injected recombinant adenovirus produced NK4 protein in vivo. In a pharmacokinetic study, the time-course changes in the concentrations of NK4 protein in the plasma and various organs were examined by ELISA, and the results are shown in Figure 5B. After a single intramuscular injection of 5×10^8 infectious particles/mL AdCMV.NK4, the plasma concentration of NK4 protein reached a maximum at day 10 and slowly declined over the following 2 weeks. NK4 protein was also detected in the liver, kidneys, and lungs. The highest concentration of NK4 was observed in the liver as compared to that in the lungs and kidneys. Treatment with NK4 was well tolerated, and no signs of toxicity such as death or weight loss were observed (Figure 5C).

HGF-producing KMS11 and KMS34 cells (1×10^7) were transplanted subcutaneously into 5- to 6-week-old male Icr/scid mice, and a skin plasmacytoma was readily established. In 3 to 4 weeks after the inoculation, that is, when these tumors reached 100 mm^3, 5×10^8 infectious particles per milliliter adenovirus was injected into the femoral muscle on days 1 and 7. As shown in Figure 6A, the growth of tumors derived from KMS11 cells was significantly inhibited in AdCMV.NK4-injected mice compared with that in AdCMV.lacZ- or PBS-treated mice (day 30, $P < .001$). In Dex-sensitive KMS11 cells, coinjection of AdCMV.NK4 with Dex enhanced the antitumor effects of AdCMV.NK4 (day 30, $P < .001$; Figure 6A). Ad-NK4 also significantly inhibited the growth of Dex-resistant KMS34 cell tumors (day 30, $P < .05$, compared with the other 2 control groups; Figure 6B).

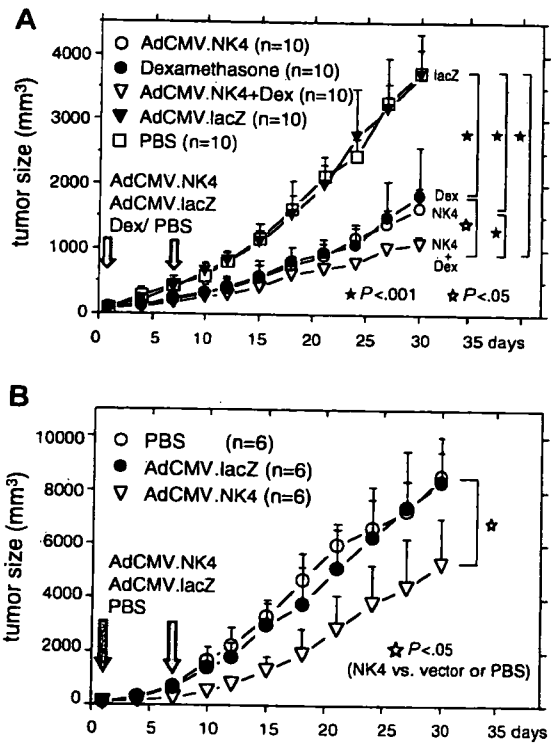

Figure 6. In vivo growth inhibition of plasmacytoma by intramuscular injection of AdCMV.NK4. A total of 1×10^7 HGF-producing KMS11 (A) and KMS34 cells (B) were inoculated subcutaneously into Icr/scid mice and a plasmacytoma was established. When the tumors reached 100 mm^3 (day 0), 5×10^8 infectious particles/mL AdCMV.NK4 or AdCMV.lacZ was injected into the femoral muscle on days 0 and 7. In Dex-sensitive KMS11 tumors, 0.8 μg/g Dex was also injected into the femoral muscle on days 0 and 7. The width and length of the plasmacytoma was measured every 3 days. Sizes on day 30 in each arm were compared and evaluated by the Student *t* test.

Histopathologic examination of MM cells treated with NK4

Subcutaneous tumors derived from KMS11 cells were isolated and microscopically observed. A significant number of MM cells exhibited signs of cell death in AdCMV.NK4-treated mice, as compared with those observed in AdCMV.lacZ- or PBS-treated mice (Figure 7A). Tumor cells treated with Dex alone also underwent extensive cell death due to the direct antimyeloma effects of Dex. TUNEL staining demonstrated that a significant number of MM cells treated with AdCMV.NK4 fell into apoptosis (Figure 7B). The microvessel density in the tumors was also evaluated by immunohistochemical staining of cross-sections with anti-VWF antibody (Figure 7C). In AdCMV.NK4-injected mice, the density of microvessels in the tumors was significantly reduced compared with that in AdCMV.lacZ-treated tumors ($P = .029$). These results, taken together with our previous observation that NK4 significantly inhibits the proliferation of endothelial cells in vitro, NK4 is considered to possess antiangiogenic activity.[15,16] The change of phosphorylation status of c-MET was also examined by immunohistochemical staining with antiphosphorylated c-MET antibody. As shown in Figure 7D, c-MET in AdCMV.NK4-treated tumors was less potently activated compared with that in AdCMV.lacZ-treated tumors.

Discussion

Coexpression of HGF and c-MET has been reported in various types of cancers.[13,20] HGF is produced by tumor cells and stromal cells and leads to the growth and metastasis of tumor cells via both autocrine and paracrine mechanisms. Figure 1 shows that in the present study, all of the myeloma cells expressed c-MET protein, and 2 cell lines also produced and secreted HGF, suggesting that the HGF–c-MET axis contributes to the growth of MM cells. Recently, it was reported that a selective c-MET tyrosine kinase inhibitor blocks HGF-induced intracellular signaling and regulates the proliferation and migration of MM cells in vitro.[21] In our study, NK4 protein also stabilized the growth of HGF-producing KMS11 and KMS34 cells in vitro as well as in vivo (Figures 2 and 6). NK4 also inhibited the growth of primary tumor cells obtained from patients with MM (Figure 2D). Immunoblot analysis revealed that NK4 inhibited the activation of HGF receptor/c-MET and the downstream signaling such as ERK1/2, STAT3, and AKT-1 in the presence or absence of HGF (Figure 4). Thus, the NK4 molecule is considered to directly regulate the proliferation of MM cells, presumably by interfering with autocrine and paracrine loops.

Growth suppression was also observed in non–HGF-producing cells such as KMS27 cells, as determined by an MTT assay conducted in HGF-free medium even though c-MET activation was weakly decreased by NK4 treatment (Figures 2A and 4). Addition of an excess amount of HGF to KMS27 cells only partially inhibited NK4-induced apoptosis, whereas HGF clearly blocked apoptosis induced by neutralizing antibody (Figure 3). In our previous reports, NK4 was shown to inhibit the proliferation of endothelial cells stimulated not only by HGF, but also by VEGF and FGF-2, even though NK4 does not inhibit the binding of VEGF or FGF-2 to their respective receptors.[16] KMS27 and other cells have been shown to produce and secrete VEGF or FGF-2 into culture medium (Y.H., unpublished data, March 2002). Subsequent study has also demonstrated that a deletion mutant of NK4 in the N-terminal hairpin domain lost HGF antagonist activity, but still inhibited the proliferation and migration of endothelial cells induced by VEGF, FGF-2, and HGF.[15] It is speculated that the biologic activities of

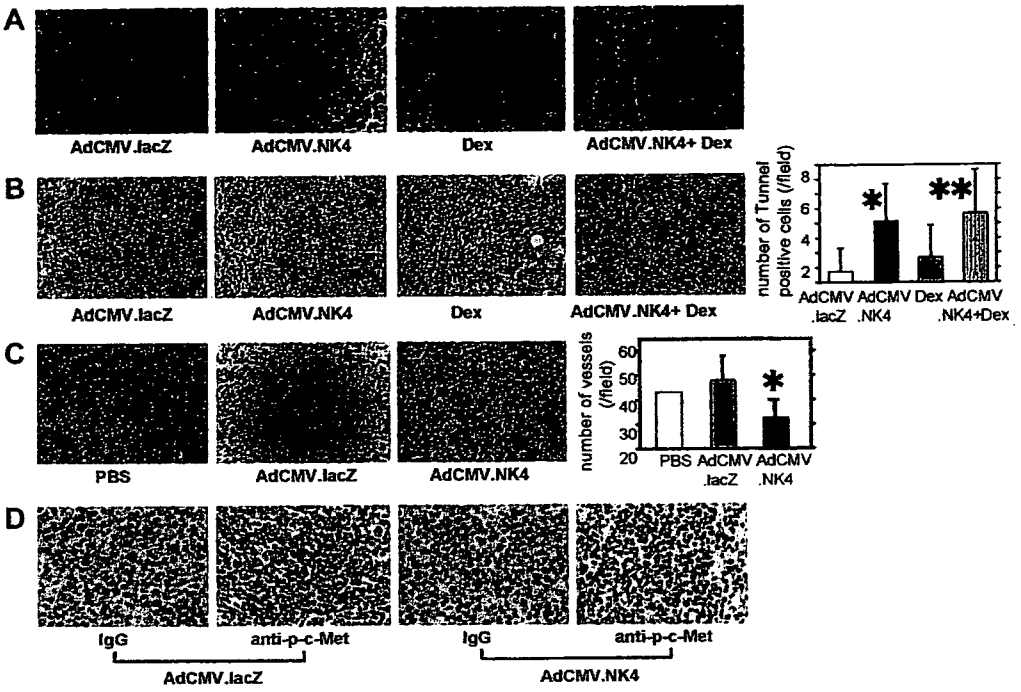

Figure 7. Histopathologic examination of KMS11-derived tumors treated with AdCMV.NK4. (A) Hematoxylin and eosin staining of AdCMV.lacZ-treated, AdCMV.NK4-treated, Dex-treated, and AdCMV.NK4 plus Dex-treated KMS11 tumors. The arrows indicate areas of tumor cell death. (B) TUNEL assay of KMS11 tumors. The numbers of TUNEL$^+$ cells per one visual field (0.148 mm^2) were counted and shown in the form of a bar graph. * $P = .001$, ** $P = .008$ compared with AdCMV.lacZ-treated tumors. (C) Immunohistochemical analysis of blood vessels in subcutaneous tumors derived from KMS11 cells. Vascular endothelial cells were stained with anti-VWF antibody. The mean number of blood vessels per one visual field is indicated by the bar graph. *$P = .029$ compared with that in AdCMV.lacZ-treated tumors. (D) Immunohistochemical staining of activated c-Met in AdCMV.NK4-treated tumors using anti–phosphorylated c-MET. To eliminate background staining, human IgG was used as a control. In panels B and C the mean ± 1 SD (n-7 for B and n-5 for C) is shown.

NK4 involve not only the antagonism of HGF/c-Met interactions, but also the inhibition of an HGF/c-Met–independent pathway. Thus, NK4 is likely bifunctional.[13] Association of NK4 to a putative binding molecule other than c-Met receptor may participate in the signal transduction for the growth inhibition of endothelial cells by NK4. However, the precise molecular mechanisms of the latter activity remain to be determined. Taken together, we speculate that the similar activity, as seen in case of endothelial inhibition, may be involved in inhibitory effect of NK4 on proliferation of MM cells.

In previous studies, it has been reported that vascular endothelial cells express c-Met and HGF induces the proliferation of endothelial cells, suggesting that HGF contributes to tumor angiogenesis.[16] Recently, a positive correlation between serum HGF concentration and bone marrow microvessel density was reported in patients with MM.[22] NK4 is structurally similar to angiostatin, a potent angiogenesis inhibitor, and previous reports have demonstrated that NK4 inhibits endothelial cell growth.[14,16,18,19,23] In the present study, a significant decrease in vascular endothelial cells in tumors was observed in AdCMV.NK4-treated mice. Thus, antiangiogenesis is expected to be among the reasons for the antimyeloma effects of NK4 in vivo.

Glucocorticoid is a key drug in the treatment of MM and is included in most of the currently applied chemotherapeutic regimens. To establish a more effective antimyeloma therapy, we examined the effects of NK4 on glucocorticoid-resistant MM cells, as well as the effects of a combination treatment using NK4 together with glucocorticoid in glucocorticoid-sensitive cells. The present in vitro and in vivo studies revealed that NK4 is effective at regulating the growth of Dex-resistant KMS34 cells. In future clinical trials, it will be worthwhile to attempt using NK4 to treat patients with MM resistant to conventional chemotherapy. As shown in Figures 2C and 6A, NK4 enhanced the antimyeloma effect of Dex in Dex-sensitive KMS11 cells in vitro as well as in vivo. Thus, NK4 treatment in combination with Dex or with another therapeutic approach may be more efficient at achieving antitumor effects. Along these lines, a previous study has already demonstrated that a combination of NK4 administration with immunotherapy using dendritic cells was effective at countering B-cell malignancy.[24]

Here, mice were exposed to a challenge with an injection of adenovirus containing NK4 cDNA into a femoral muscle remote from the tumor; the findings demonstrated the systemic delivery of secreted NK4 protein, which in turn led to antimyeloma effects in vivo. In addition, AdCMV.NK4-treated mice did not show any weight loss (Figure 5C) or features of significant tissue damage (eg, venous thrombosis), as based on both macroscopic and microscopic observations (data not shown). These results suggest the feasibility of NK4 gene therapy for patients with MM. Indeed, the tissue and plasma concentrations of NK4 were less than 1 ng/mL. Kushibiki and colleagues also demonstrated the antitumor activities of NK4 using a plasmid vector system in breast cancer-bearing mice, even though the plasma concentration of NK4 was much lower in their model than that observed in our model.[25] Even at low concentrations, the long-term exposure of tumor cells to NK4 may delay the growth of tumor cells. In addition, NK4 exhibited antimyeloma effects via multiple mechanisms in vivo; for example, not only direct antitumor effects such as serving as an HGF antagonist, but also antiangiogenic effects and unknown HGF-independent mechanisms were suggested as putative mechanisms, as discussed above in this section. According to the sum effects of these mechanisms, NK4 might have significantly inhibited the proliferation of MM cells inoculated into the SCID mice, even though only low plasma concentrations were achieved.

With the aim of improving future clinical applications, additional studies of the biologic effects of NK4 should be carried out, in particular those involving normal tissues. Alternative safe methods for the delivery

of the NK4 gene or gene products should be also explored, including the administration of synthetic NK4 peptide.

Acknowledgments

This work was supported by grants from the International Myeloma Foundation Aki Horinouchi Research Grant (Y.H.) and Keio Gijuku Academic Development Funds (Y.H.).

Authorship

Contribution: Y.H. designed the study, performed all in vitro and in vivo experiments, analyzed data, wrote the paper, and had all responsibility for this manuscript; W.D. and T.Y. helped with histopathologic examinations; K.M. and T. Nakamura provided the NK4 protein and recombinant adenovirus, and they also helped with the analyzing the data and writing the manuscript; M.S. helped with the FACS study; T.O. provided the myeloma cell lines; T. Niikura contributed to the preparation of the recombinant adenovirus; T. Nukiwa established and provided the recombinant adenovirus; and Y.I. supervised the experiments, data analysis, and provided critical revision of the manuscript.

Conflict-of-interest disclosure: The authors declare no competing financial interests.

Correspondence: Yutaka Hattori, Division of Hematology, Department of Internal Medicine, Keio University School of Medicine, 35 Shinanomachi, Shinjuku-ku, Tokyo 160-8582, Japan; e-mail: yhattori@sc.itc.keio.ac.jp.

References

1. Alexanian R, Dimopoulos M. The treatment of multiple myeloma. N Engl J Med. 1994;330:484-489.
2. Vacca, A, Ribiatti D, Presta M, et al. Bone marrow neovascularization, plasma cell angiogenic potential, and matrix metalloproteinase-2 secretion parallel progression of human multiple myeloma. Blood. 1999;93:3064-3073.
3. Du W, Hattori Y, Hashiguchi A, et al. Tumor angiogenesis in the bone marrow of multiple myeloma patients and its alteration by thalidomide treatment. Pathol Int. 2004;54:285-294.
4. Sezer O, Jakob C, Eucker J, et al. Serum levels of the angiogenic cytokines basic fibroblast growth factor, vascular endothelial growth factor and hepatocyte growth factor in multiple myeloma. Eur J Haematol. 2001;66:83-88.
5. Sato N, Hattori Y, Wenlin D, et al. Elevated level of plasma basic fibroblast growth factor in multiple myeloma correlates with increased disease activity. Jpn J Cancer Res. 2002;93:459-466.
6. Borset M, Hjorth-Hansen H, Seidel C, Sundan A, Waage A. Hepatocyte growth factor and its receptor c-met in multiple myeloma. Blood. 1996;88: 3998-4004.
7. Iwasaki T, Hamano T, Ogata A, et al. Clinical significance of vascular endothelial growth factor and hepatocyte growth factor in multiple myeloma. Br J Haematol. 2002;116:796-802.
8. Seidel C, Borset M, Turesson I, et al. Elevated serum concentrations of hepatocyte growth factor in patients with multiple myeloma. The Nordic Myeloma Study Group. Blood. 1998;91:806-812.
9. Seidel C, Lenhoff S, Brabrand S, et al, for the Nordic Myeloma Study Group. Hepatocyte growth factor in myeloma patients treated with high-dose chemotherapy. Br J Haematol. 2002; 119:672-676.
10. Derksen PWK, Keehnen RM, Evers LM, et al. Cell surface proteoglycan syndecan-1 mediates hepatocyte growth factor binding and promotes Met signaling in multiple myeloma. Blood. 2002; 99:1405-1410.
11. Date K, Matsumoto K, Shimura H, Tanaka M, Nakamura T. HGF/NK4 is a specific antagonist for pleiotrophic actions of hepatocyte growth factor. FEBS Lett. 1997;420:1-6.
12. Date K, Matsumoto K, Kuba K, et al. Inhibition of tumor growth and invasion by a four-kringle antagonist (HGF/NK4) for hepatocyte growth factor. Oncogene. 1998;17:3045-3054.
13. Matsumoto K, Nakamura T. Mechanisms and significance of bifunctional NK4 in cancer treatment. Biochem Biophys Res Commun. 2005 ;333:316-327.
14. O'Reilly MS, Holmgren L, Shing Y, et al. Angiostatin: a novel angiogenesis inhibitor that mediates the suppression of metastases by a Lewis lung carcinoma. Cell 1994;79:315-328.
15. Kuba K, Matsumoto K, Ohnishi K, et al. Kringle 1-4 of hepatocyte growth factor inhibits proliferation and migration of human microvascular endothelial cells. Biochem Biophys Res Commun. 2000 ;279:846-852.
16. Kuba K, Matsumoto K, Date K, et al. HGF/NK4, a four-kringle antagonist of hepatocyte growth factor, is an angiogenesis inhibitor that suppresses tumor growth and metastasis in mice. Cancer Res. 2000 ;60:6737-6743.
17. Otsuki T, Yamada O, Yata K, et al. Expression of fibroblast growth factor and FGF-receptor family genes in human myeloma cells, including lines possessing t(4;14)(q16.3;q32.3) and FGFR3 translocation. Int J Oncol. 1999;15:1205-1212.
18. Tomioka D, Maehara N, Kuba K, et al. Inhibition of growth, invasion, and metastasis of human pancreatic carcinoma cells by NK4 in an orthotopic mouse model. Cancer Res. 2001;61:7518-7524.
19. Maemondo M, Narumi K, Saijo Y, et al. Targeting angiogenesis and HGF function using an adenoviral vector expressing the HGF antagonist NK4 for cancer therapy. Mol Ther. 2002;5:177-185.
20. Jiang WG, Hiscox S, Matsumoto K, Nakamura T. Hepatocyte growth factor/ scatter factor, its molecular, cellular and clinical implications in cancer. Crit Rev Oncol Hematol. 1999;29:209-248.
21. Hov H, Holt RU, Ro T B, et al. A selective c-Met inhibitor blocks an autocrine hepatocyte growth factor loop in ANBL-6 cells and prevents migration and adhesion of myeloma cells. Clin Cancer Res. 2004;10: 6686-6694.
22. Andersen NF, Standal T, Nielsen JL, et al. Syndecan-1 and angiogenic cytokines in multiple myeloma: correlation with bone marrow angiogenesis and survival. Br J Haematol. 2005;128:210-217.
23. Wen J, Matsumoto K, Taniura N, Tomioka D, Nakamura T. Hepatic gene expression of NK4, an HGF-antagonist/angiogenesis inhibitor, suppresses liver metastasis and invasive growth of colon cancer in mice. Cancer Gene Ther. 2004; 11:419-430.
24. Kikuchi T, Maemondo M, Narumi K, et al. Tumor suppression induced by intratumor administration of adenovirus vector expressing NK4, a 4-kringle antagonist of hepatocyte growth factor, and naive dendritic cells. Blood 2002;100:3950-3959.
25. Kushibiki T, Matsumoto K, Nakamura T, Tabata Y. Suppression of the progress of disseminated pancreatic cancer cells by NK4 plasmid DNA released from cationized gelatin microspheres. Pharm Res. 2004;21:1109-1118.

Establishment of Perineural Invasion Models and Analysis of Gene Expression Revealed an Invariant Chain (CD74) as a Possible Molecule Involved in Perineural Invasion in Pancreatic Cancer

Norimasa Koide,[1,5] Taketo Yamada,[1] Rie Shibata,[1] Taisuke Mori,[1] Mariko Fukuma,[1] Ken Yamazaki,[1,3] Koichi Aiura,[2] Motohide Shimazu,[2] Setsuo Hirohashi,[4] Yuji Nimura,[5] and Michiie Sakamoto[1]

Abstract

Purpose: Perineural invasion causes frequent local recurrence even after resection and a poor prognosis for pancreatic cancer. We established perineural invasion models and analyzed the molecular mechanism of perineural invasion in pancreatic cancer.

Experimental Design: Seven pancreatic cancer cell lines with or without human peripheral nerves were s.c. implanted in nonobese diabetes/severe combined immunodeficient mice. We compared expression profiles among high and low perineural invasion cell lines by using an oligonucleotide microarray. We examined up-regulation of the invariant chain (CD74) in high perineural invasion cell lines in mRNA and protein levels and surgical cases immunohistochemically.

Results: Four of seven pancreatic cancer cell lines (CaPan1, CaPan2, CFPAC, and MPanc96) showed perineural invasion to s.c. transplanted human peripheral nerves. Moreover, CaPan1 and CaPan2 (high perineural invasion group) also resulted in a high frequency of perineural invasion to mouse s.c. peripheral nerves, whereas three pancreatic cancer cell lines HPAFII, AsPC1, and Panc1 (low perineural invasion group) did not show perineural invasion to either human or mouse nerves. We identified 37 up-regulated genes and 12 down-regulated genes in the high perineural invasion group compared with the low perineural invasion group. Among them, CD74 was up-regulated in the high perineural invasion group in mRNA and protein levels. Furthermore, immunohistochemical expression of CD74 in clinical cases revealed its significant overexpression in pancreatic cancer with perineural invasion ($P < 0.008$).

Conclusions: This is the first report of perineural invasion models using human pancreatic cancer cell lines. In combination with gene expression profiling, it was indicated that CD74 could be a candidate molecule involved in perineural invasion. These models provide new approaches for study of perineural invasion in pancreatic cancer.

Pancreatic cancer is the fourth leading cause of cancer-related death in the United States (1). Worldwide pancreatic cancer causes an estimated 213,000 deaths a year (2). In the United States, ~32,180 patients are diagnosed with pancreatic cancer annually, and nearly an equal number will die from the disease (1). When first diagnosed with pancreatic cancer, about 80% of all patients receive palliative therapy instead of surgery because of locally advanced disease, depending on perineural invasion or metastasis. The remaining 20% of patients receiving surgery still have a poor prognosis due to high incidence and early occurrence of local recurrence and hepatic and lymph node metastasis, even after pathologically curative surgery (3–5). It is suspected that microscopic hepatic metastasis is already present (6). Cancer cells spreading in the perineural space even at an early clinical stage also cause local recurrence in the retroperitoneum because of residual tumor cells in the perineural space after surgical resection (7). Moreover, many previous clinicopathologic reports showed that perineural invasion in pancreatic cancer was one of the most significant poor prognostic factors (8, 9).

Genetic alternations seem to be responsible for the development of pancreatic cancer (10). Recently, pancreatic cancer–specific expression profiles using cDNA microarrays (11–13), Affymetrix gene chip (14, 15), and serial analysis of gene expression (16) have been used by many investigators. However, the molecular mechanisms of hepatic metastasis and perineural invasion in pancreatic cancer are far from clear. Some studies reported metastasis-related genes by analyzing gene expression profiles between a highly metastatic variant and a parental pancreatic cancer cell line in an orthotopic

Authors' Affiliations: Departments of [1]Pathology and [2]Surgery, School of Medicine, Keio University; [3]Genomic Division and [4]Pathology Division, National Cancer Center Research Institute, Tokyo, Japan; and [5]Division of Surgical Oncology, Department of Surgery, Nagoya University, Nagoya, Japan

Received 8/23/05; revised 1/12/06; accepted 2/2/06.

Grant support: Grant-in-aid for the 21th Century Center of Excellence program and Cancer Research from the Ministry of Education, Culture, Sports, Science and Technology of Japan, for the Third Term Comprehensive 10-Year Strategy for Cancer Control from the Ministry of Health, Labor and Welfare of Japan, and for Cancer Research from the Foundation for Promotion of Cancer Research.

The costs of publication of this article were defrayed in part by the payment of page charges. This article must therefore be hereby marked *advertisement* in accordance with 18 U.S.C. Section 1734 solely to indicate this fact.

Requests for reprints: Michiie Sakamoto, Department of Pathology, School of Medicine, Keio University, 35 Shinanomachi, Shinjyuku-ku, Tokyo, 160-8582, Japan. Phone: 81-3-5363-3764; Fax: 81-03-3353-3290; E-mail: msakamot@sc.itc.keio.ac.jp.

doi:10.1158/1078-0432.CCR-05-1852

transplanted nude mouse model (17, 18). However, there are few reports about the molecular mechanisms of perineural invasion of pancreatic cancer due to the lack of good disease models. Understanding perineural invasion at the molecular level is an important step towards the identification of prognostic markers and therapeutic targets for pancreatic cancer treatment.

To analyze the mechanisms of perineural invasion in pancreatic cancer, we constructed perineural invasion models using s.c. implantation of human pancreatic cancer cell lines. CaPan1 and CaPan2 (high perineural invasion group) implanted s.c. into nonobese diabetes/severe combined immunodeficient (NOD/SCID) mice were frequently found to form perineural invasion to the mouse s.c. nerves and transplanted human nerves, whereas three pancreatic cancer cell lines HPAFII, AsPC1, and Panc1 (low perineural invasion group) did not show perineural invasion to either human or mouse nerves. Next, we compared gene expression profiles between the high and low perineural invasion groups using a microarray technique. Of these genes, we further investigated whether *invariant chain* (*CD74*) expression was associated with perineural invasion.

Materials and Methods

Cell culture. The human pancreatic cancer cell lines CaPan1, CaPan2, HPAFII, AsPC1, Panc1, CFPAC, and MPanc96 were obtained from the American Type Culture Collection (Manassas, VA). All cell lines were cultured in RPMI 1640 (Sigma, St. Louis, MO) containing 10% heat-inactivated fetal bovine serum, 100 μg/mL ampicillin, and 100 μg/mL streptomycin. All cell cultures were done at 37°C under 5% CO_2.

Perineural invasion models in mice. NOD/SCID (NOD/LtSz-scid) mice were maintained in a specific pathogen-free environment. Eight- to 12-week-old mice were used in this experiment. The studies were conducted in accordance with the NIH Guide for the Care and Use of Laboratory Animals.

The human nerve perineural invasion models were prepared as follows. The human nerve plexus around the celiac axis or superior mesenteric artery were obtained from autopsies done until about 6 hours after death in sterile conditions, immediately placed in RPMI 1640 with antibiotics, divided into 1-cm pieces (about 0.25 cm^3), and kept in the medium for a brief period until transplantation. The divided tissue was placed in the s.c. space of NOD/SCID mice under anesthesia. After 4 weeks, each mouse received an injection of a pancreatic cancer cell line near the s.c. transplanted tissue with 7×10^6 viable tumor cells, which were harvested from subconfluent cultures, under the appropriate anesthetic procedure. Five to 8 weeks later, when the tumor grew up to about 1.5 cm in long diameter, after inoculation, mice were sacrificed, and autopsies were done immediately. The s.c. tissue was removed, fixed in 10% formalin, cut into 2- to 3-mm-thick slices, and embedded in paraffin. The samples were processed for histologic examination.

The mouse nerve perineural invasion models were prepared as follows. Each mouse received a s.c. injection of 7×10^6 viable pancreatic cancer cells on the midline of the mouse's back and processed by the same protocol as above. All animals tolerated each procedure well.

RNA preparation and oligonucleotide array. Total RNA was extracted from cells with an RNAeasy Mini kit (Qiagen, Hilden, Germany). According to the manufacturer's protocol (Affymetrix, Santa Clara, CA), biotin-labeled cRNA was synthesized from 5 mg of total RNA, hybridized to the GeneChip HG-U133A, stained with streptavidin-phycoerythrin, and then detected by scanning. Each of the scanned images was normalized as mean signal intensity of all probe sets at 1,000. Two-dimensional clustering analysis using the standard correlation as a similarity measure was done by the software, GeneSpring version 6.2 (Silicon Genetics, Redwood City, CA).

Real-time quantitative reverse transcription-PCR analysis. Real-time quantitative reverse transcription-PCR (RT-PCR) analysis was done as follows. The primer set 5′-GACCTTATCTCCAACAATGAGCAAC-3′ (forward) and 5′-AGCAGAGTCACCAGGATGGAA-3′ (reverse) was used for CD74. To standardize the amount of RNA, expression of

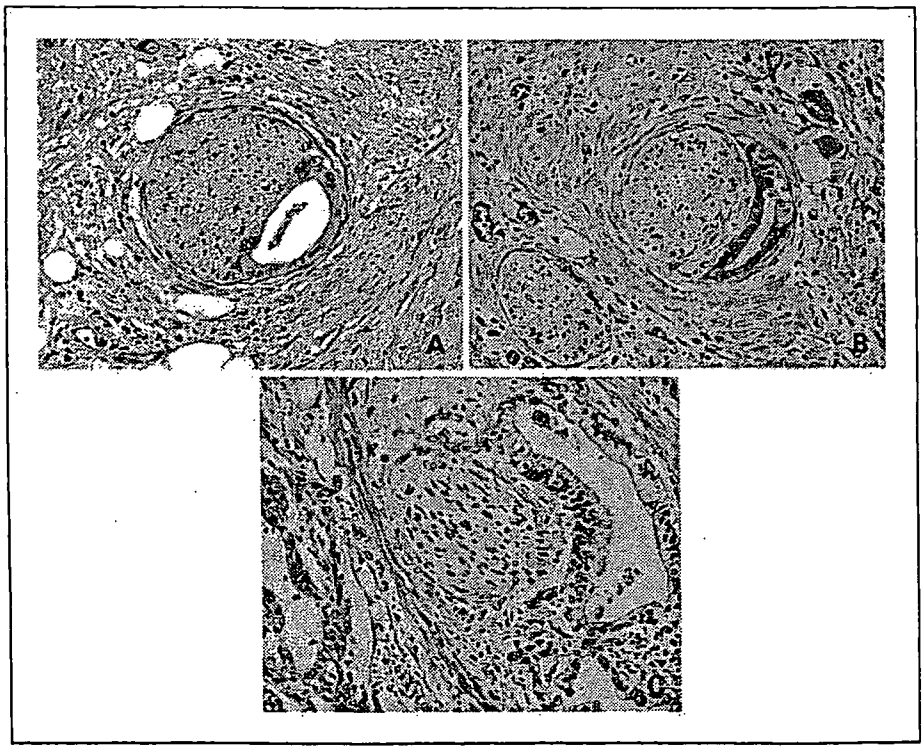

Fig. 1. Three patterns of relationships between cancer cells and peripheral nerves. Perineural invasion: cancer cells invaded to the perineural space between the perineurium and endoneurium of the peripheral nerve with direct contact with the endoneurium (*A*). Epineural invasion: cancer cell invaded along the perineurium without contact with the endoneurium (*B*). Nerve involvement: cancer nests included nerves without direct mutual contact (*C*). H&E; magnification × 200.

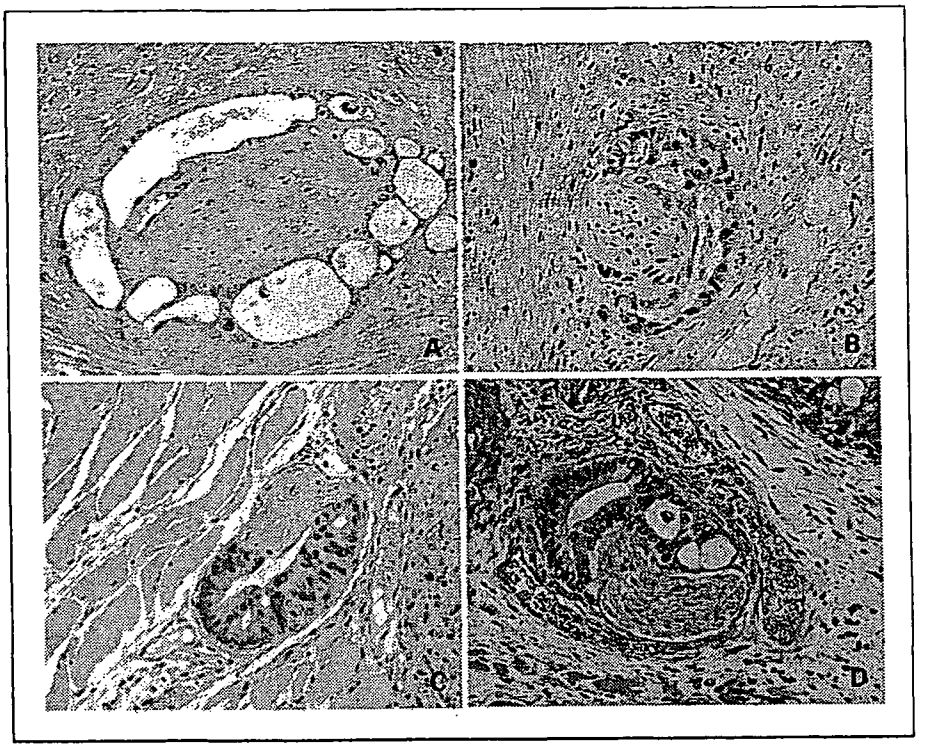

Fig. 2. Perineural invasion to human and mouse nerves. Perineural invasion in a human nerve perineural invasion model (*A*, CaPan2; *B*, CFPAC) and perineural invasion in a mouse nerve perineural invasion model (*C*, CaPan1; *D*, CaPan2). H&E; magnification × 200.

glyceraldehyde-3-phosphate dehydrogenase in each sample was quantified by using the primer set 5′-GCACCGTCAAGGCTGAGAAC-3′ (forward) and 5′-ATGGTGGTGAAGACGCCAGT-3′ (reverse), and the amount of CD74 expression was divided by that of the glyceraldehyde-3-phosphate dehydrogenase in each sample. All PCR reactions were done under the following conditions: one cycle at 95°C for 10 seconds and then 40 cycles at 95°C for 5 seconds and 60°C for 30 seconds. Real-time detection of the emission intensity of SYBR Green (Qiagen) was done using an ABI prism 7000 Sequence Detector (Perkin-Elmer Applied Biosystems, Foster city, CA), using a previously reported method (19). Quantitative RT-PCR was done at least thrice.

Western blotting. All 20-μg cell lysates were subjected to 10% SDS-PAGE and then separated proteins were transferred to Hybond-P (Amersham Biosciences, Buckinghamshire, United Kingdom). After blocking, an anti-CD74 mouse monoclonal antibody (LN 2; DAKO, Glostrup, Denmark) was used at a dilution of 1:1,000 overnight at 4°C. The membrane was incubated with a horseradish peroxidase–conjugated secondary antibody (DAKO) and visualized by using an enhanced chemiluminescence kit (Amersham Biosciences). A Burkitt's lymphoma (Raji) cell line was used as a positive control for CD74.

Immunofluorescence. CaPan2 cell lines were grown on glasses and fixed in 8% paraformaldehyde for 20 minutes on ice. They were incubated with an anti-CD74 antibody for 1 hour followed by a FITC-labeled secondary antibody (DAKO). Texas Red-X phalloidin (Molecule Probes, Eugene, OR) was used to visualize filamentous-actin. Slides were examined using an Olympus fluorescence microscope with a MRC-600 scanning laser confocal apparatus (Olympus, Tokyo, Japan).

Patients and tissue samples. For immunohistochemical analysis, 67 invasive ductal pancreas adenocarcinomas were analyzed. Sections were prepared from formalin-fixed, paraffin-embedded tissues of samples resected surgically between 1991 and 2004. This study was conducted under the approval of the Ethics Committee of Keio University, School of Medicine. Histologic diagnoses were made according to WHO criteria or the Japan pancreas society classification (20). Perineural invasion, which was frequently observed in surgical specimens, was defined as cancer cell invasion to the perineural space between the perineurium and endoneurium of the peripheral nerve with direct contact to the endoneurium (Fig. 1A), whereas epineural invasion, where cancer cells invade along the perineurium without contact to the endoneurium (Fig. 1B), and nerve involvement, where a cancer nest included nerves without direct contact between them (Fig. 1C), were excluded from perineural invasion (21). Intraneural invasion was also included in perineural invasion.

The degree of perineural invasion was defined microscopically as follows: 0, no perineural invasion; 1, perineural invasion was difficult to find with only one to three occurrences in the lesions; 2,

Table 1. Incidence of perineural invasion in mouse nerve perineural invasion models

	CaPan1	CaPan2	HPAFII	AsPC1	Panc1	*P**
No. mice examined	11	13	11	11	5	
Perineural invasion	6†	9	0	0	0	0.000004
Epineural invasion	3	6	3	4	0	0.216
Nerve involvement	6	8	5	7	3	0.615

*CaPan1 and CaPan2 vs HPAFII, AsPC1, and Panc1.
†Each value indicates the number of mice where perineural invasion, epineural invasion, and nerve involvement was observed, respectively.

perineural invasion was easy to find, in between 1 and 3; and 3, perineural invasion was even easier to find, with more massive occurrences in the lesions and extension beyond the border of the main tumor mass.

Immunohistochemistry. Each section was deparaffinized, rehydrated, and incubated with fresh 0.3% hydrogen peroxide in methanol for 30 minutes at room temperature and then heated in 10 mmol/L citrate buffer (pH 6) for 10 minutes after washing in PBS. Normal goat serum (Invitrogen, Carlsbad, CA) was applied for 30 minutes and removed. The section was then incubated with anti-CD74 antibody at a dilution of 1:100 overnight at 4°C, washed thrice in PBS, and incubated with a secondary antibody for 30 minutes at room temperature. A simple stain MAX-PO (Nichirei, Tokyo, Japan) was used to detect the antibody signals as the secondary antibody. Staining was evaluated by three independent observers (N.K., R.S., and M.S.). An equal staining to lymphocytes was considered positive. The positivity index was expressed as the percentage of positive cancer cells in each lesion. The cases with ≥10% positive cells were defined as CD74 positive.

Statistical analysis. Data are expressed as mean ± SD. The level of CD74 mRNA in the high and low perineural invasion groups was compared using the Mann-Whitney *U* test. The other correlations were analyzed by the χ^2 test. All statistical analyses were done using Statcel2 (OMS Publisher, Saitama, Japan). The results were judged significant at $P < 0.05$.

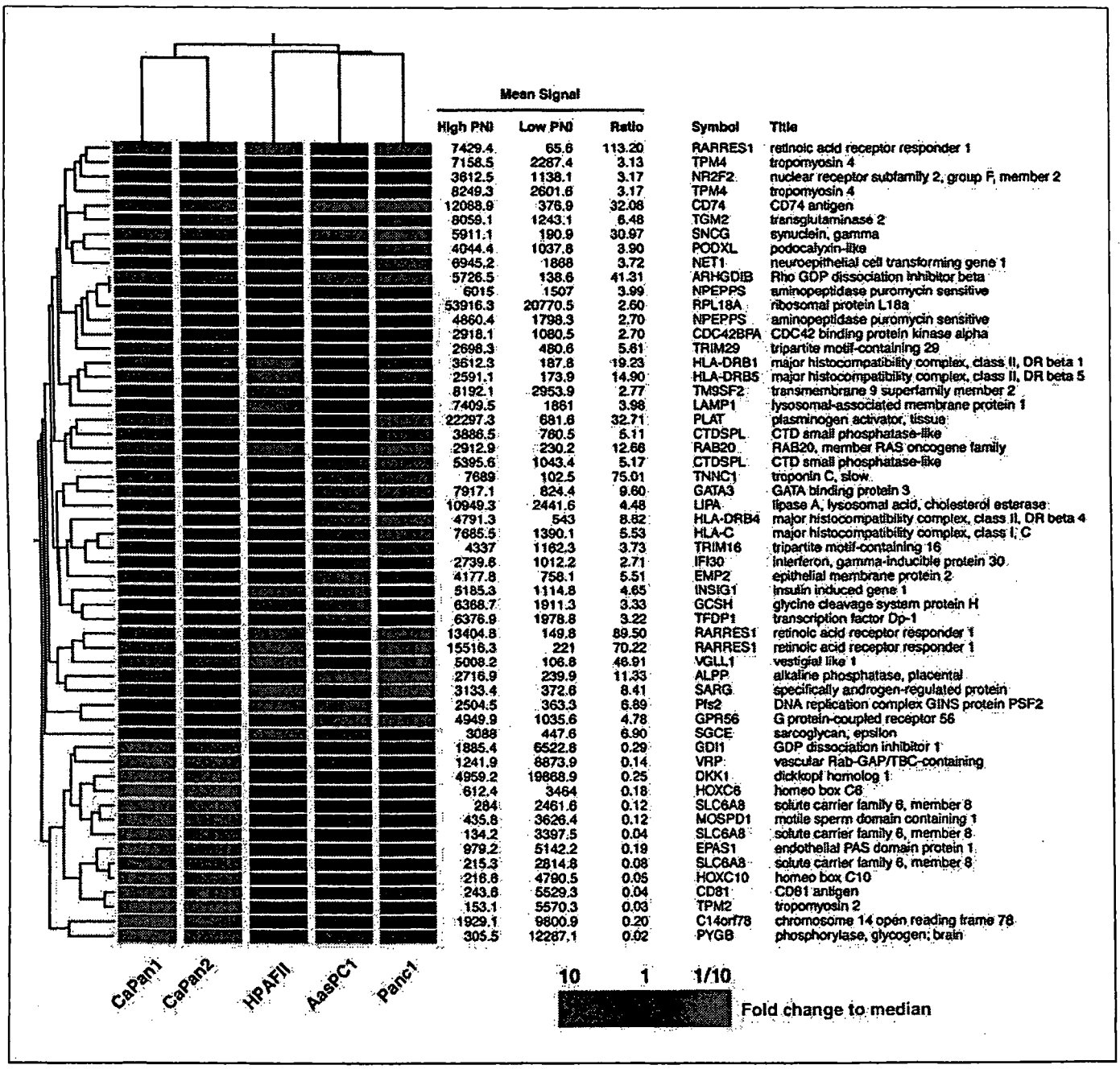

Fig. 3. Two-way hierarchical clustering algolithm. Forty-nine genes displayed a ≥2-fold increase or decrease in expression level. Each color patch in the resulting visual map represents the expression level of the associated gene in the cell line sample, with a continuum of expression levels from *green* (lowest) to *bright red* (highest). A two-way hierarchical clustering algorithm successfully distinguished between the high and low perineural invasion groups. The scale bar reflects the fold increase (*red*) or decrease (*green*) for any given gene relative to the median level of expression across all samples.

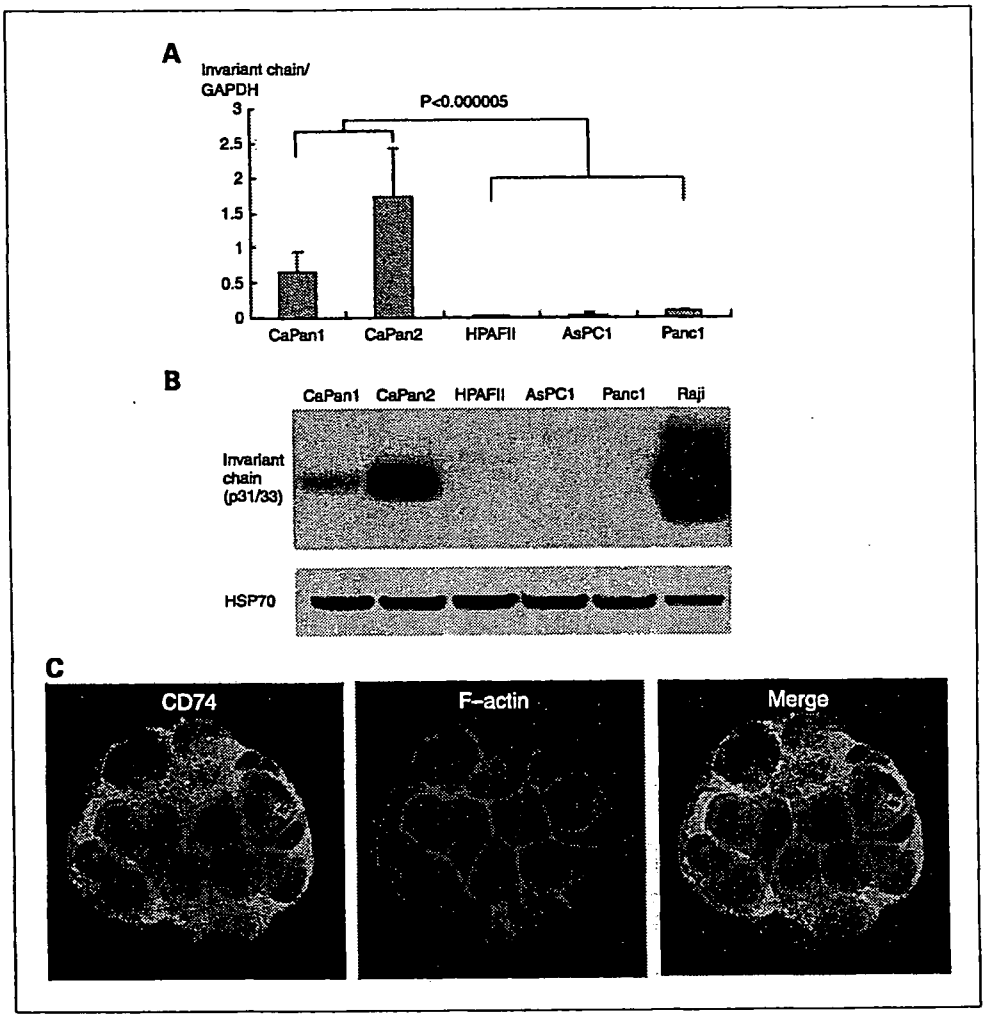

Fig. 4. CD74 expression in pancreatic cancer cell lines. *A*, real-time quantitative RT-PCR analysis of CD74. The expression levels were normalized with glyceraldehyde-3-phosphate dehydrogenase (*GAPDH*) mRNA in each sample. *B*, Western blotting analysis of the CD74 protein. Each cell lysate (20 μg) was analyzed using an anti-CD74 antibody. HSP70 was used as an internal control. *C*, immunofluorescence analysis of CD74 and filamentous actin (*F-actin*) in CaPan2. CaPan2 cells were stained for CD74 (*green*) and filamentous actin (*red*).

Results

Subcutaneous implantation of pancreatic cancer cell lines. To analyze the potential of perineural invasion, seven pancreatic cancer cell lines were s.c. implanted in NOD/SCID mice with human nerve tissue. CaPan1, CaPan2, CFPAC, and MPanc96 showed perineural invasion to human nerves (Fig. 2A and B). Therefore, we confirmed that even cell lines preserved their ability to show perineural invasion to human nerve-like clinical cases. However, pancreatic cancer cell lines frequently did not invade to the transplanted human nerve tissue, probably due to the adverse effect of accompanying inflammatory cells in nerve tissue. Thus, it was difficult to evaluate these models quantitatively. Because we observed these cells also presented perineural invasion to mouse s.c. peripheral nerves (Fig. 2C and D), we employed mouse nerve perineural invasion models for further analyses of perineural invasion.

To analyze quantitatively the frequency of perineural invasion of pancreatic cancer cell lines in mouse s.c. nerves, we selected five cell lines (CaPan1, CaPan2, HPAFII, AsPC1, and Panc1) and implanted these cell lines in the s.c. tissue of 5 to 13 NOD/SCID mice and analyzed the frequency of neural invasion to the mouse s.c. nerves. Perineural invasion of CaPan1 and CaPan2 cells was seen in 6 of 11 and 9 of 13 implanted mice, respectively. In contrast, the other three cell lines did not show perineural invasion, whereas each cell line showed epineural invasion and nerve involvement to the mouse s.c. nerves. These findings indicated that CaPan1 and CaPan2 (high perineural invasion group) had greater potential for perineural invasion *in vivo*, whereas the other three cell lines (low perineural invasion group) had little potential for perineural invasion ($P < 0.000004$; Table 1).

Two-way hierarchical clustering algorithm. To identify genes generally involved in perineural invasion, we compared the expression profiles of the high and low perineural invasion groups. We filtered all genes, with the following limits: (*a*) presence with signal at >2,000; (*b*) >2-fold increase or decrease in average difference between each high perineural invasion cell line and the low perineural invasion group and the high perineural invasion group and each low perineural invasion cell line. In the 49 genes selected under the above criteria, 37 were up-regulated, and 12 were down-regulated in the high perineural invasion group compared with the low perineural invasion group. A two-way hierarchical clustering algorithm successfully distinguished between the high and low perineural invasion groups (Fig. 3).

CD74 expression in pancreatic cancer cell lines. From the genes listed in Fig. 3, we further investigated *CD74*, because it was one of the most highly expressed genes in the high perineural invasion group and is thought to be a membrane

protein that might mediate cancer cell-nerve interaction. To confirm overexpression of CD74 in the high perineural invasion group, we analyzed the level of CD74 mRNA by real-time quantitative RT-PCR. The average relative expression level of CD74 (CD74/glyceraldehyde-3-phosphate dehydrogenase) was significantly higher in the high perineural invasion group than in the low perineural invasion group ($P < 0.000005$), although CaPan1 expressed less CD74 than CaPan2 (Fig. 4A). Next, we used an antibody against CD74 to investigate protein expression of CD74 in five pancreatic cancer cell lines. As in the RT-PCR analysis, CaPan2 and CaPan1 showed significantly higher expression of CD74 than the low perineural invasion group (Fig. 4B). Immunocytochemically, CD74 expression in CaPan2 was found on the cell surface and also more intensely in the cytoplasm (Fig. 4C). Immunohistochemical expression of CD74 in mouse s.c. tumors of these cell lines also showed a similar expression pattern and confirmed the usefulness of the CD74 antibody in immunohistochemistry (Fig. 5A).

Immunohistochemical expression of CD74 in pancreatic cancer tissues. To determine whether CD74 is also overexpressed at the protein level in human pancreatic cancer tissues and involved in perineural invasion, we examined CD74 expression in the surgical cases with an immunohistochemical study. Pancreatic ducts in noncancerous tissues of the normal pancreas or chronic pancreatitis were almost negative or focal immunostaining. However, the lymphocytes always stained strongly and thus served as an internal control of positive staining (Fig. 5B). Neural tissue and acinar cells also showed moderate staining focally. Some pancreatic cancer without perineural invasion showed little or moderate CD74 immunoreactivity, whereas pancreatic cancer with perineural invasion tended to show strong CD74 immunoreactivity (Fig. 5C and D). Strong immunoreactivity was generally observed in the cytoplasm (granular or diffuse) and sometime along the cell membranes of cancer cells. We evaluated the relationship between CD74 and clinicopathologic features. Table 2 shows that degree of perineural invasion was significantly associated with CD74 expression ($P < 0.008$). Other clinicopathologic factors were not associated with CD74 expression, although it seemed to decrease with age ($P < 0.025$).

Discussion

Perineural invasion, together with liver metastasis, is one of the poorest prognostic factors after curative resection (22, 23). Many studies on the perineural invasion of pancreatic cancer and other cancers were clinocopathologic studies using surgical specimens or molecular studies associated with neurotrophins (21, 24–28). Recently, *in vitro* models of perineural invasion using prostate cancer cell lines and mouse dorsal nerves were reported and suggested to be useful to investigate the mechanism of perineural invasion *in vitro* (29, 30). In the present study, we successfully established a perineural invasion model *in vivo* for the first time. We transplanted normal human peripheral nerves into NOD/SCID mice because these mice are an excellent tool to establish human tissue-specific metastasis models (31, 32). As expected, nerve tissues were intact even about 100 days after transplantation. In addition, we showed that pancreatic cancer cell lines preserved their ability of perineural invasion to human nerves. Moreover, they had the ability of perineural invasion to mouse s.c. nerve, too. Finally, using a mouse nerve perineural invasion model, we could clearly separate the high and low perineural invasion groups.

To elucidate the characteristic changes associated with perineural invasion, we globally analyzed the gene expression in the high and low perineural invasion groups. Among up-genes, we further investigated the CD74 molecule and

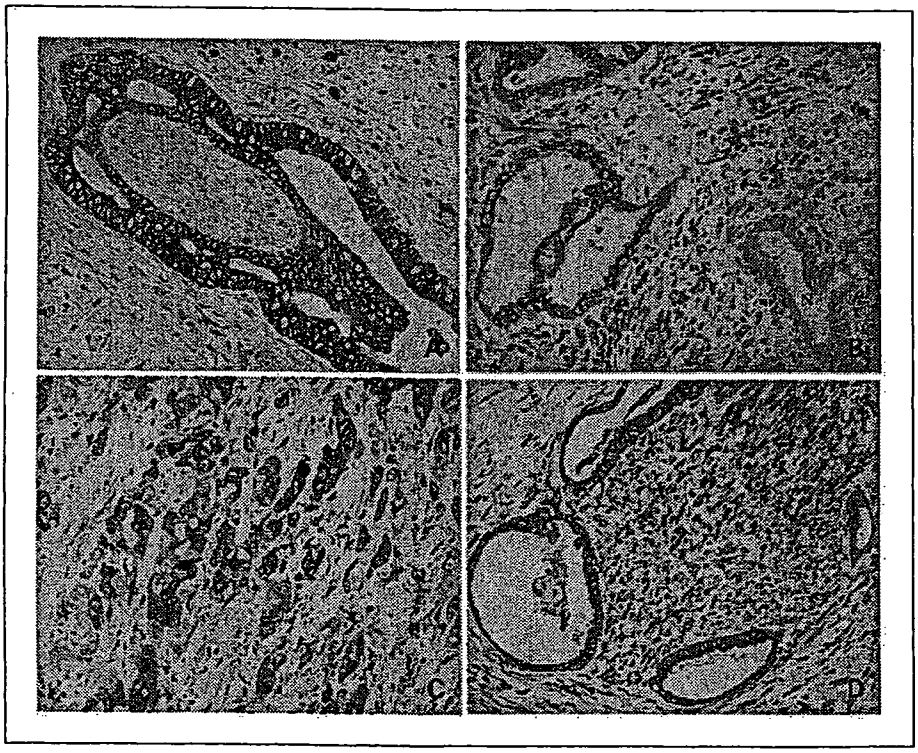

Fig. 5. Immunohistochmical staining of CD74. *A*, CD74 was diffusely expressed in the cytoplasm and cell membrane of CaPan2 demonstrating perineural invasion. *B*, CD74 was negative in the normal pancreatic duct (*N*) but strongly positive in cancer cells and lymphocytes. CD74 was diffusely expressed in poorly differentiated (*C*, perineural invasion 3) and well differentiated (*D*, perineural invasion 3) pancreatic cancer with perineural invasion. Magnification × 200.

Table 2. Immunohistochemical examination of CD74 in human pancreatic cancer tissues

	CD74 expression		P
	−	+	
No. cases	15	52	
Mean age (y)	70.5 ± 9.3	63.9 ± 9.6	0.025
Sex			
Male	10	34	0.9267
Female	5	18	
Differentiation			
Well	7	17	0.499
Intermediate	7	33	
Poor	1	2	
Stroma			
Medullary	0	0	0.622
Intermediate	5	21	
Scirrhous	10	31	
INF			
α	0	0	0.718
β	5	20	
γ	10	32	
Lymphatic invasion			
0-1	11	25	0.073
2-3	4	28	
Lymph node metastasis			
Absent	8	14	0.055
Present	7	38	
Vascular invasion			
0-1	10	24	0.161
2-3	5	28	
Perineural invasion			
0-1	10	15	0.008
2-3	5	37	

confirmed its overexpression in pancreatic cancer and association with perineural invasion. Because two cell lines in high perineural invasion group are better differentiated than three cell lines in low perineural invasion group (33), some of the selected genes might represent tumor differentiation but not perineural invasion. However, it was not likely in case of CD74, because there was no correlation between CD74 expression and tumor differentiation in tumor specimens.

CD74 was originally identified as a γ chain that is associated with the α and β chains of HLA-DR (MHC class II). Many studies have shown that CD74 plays an important role in the assembly, transport, and loading of peptides by HLA-DR molecules. HLA-DR and CD74 interacted in the endoplasmic reticulum immediately after their synthesis. This interaction of CD74 prevented binding by HLA-DR molecules to endogenous peptides (34). This was initially observed on antigen-presenting cells, but recently, it was reported that some malignant cells also expressed CD74, suggesting that CD74 expression might prevent presentation of tumor antigens (35–37). Moreover, preclinical studies in B-cell lymphoma and multiple myeloma showed CD74 was a novel and promising therapeutic target because binding of anti-CD74 monoclonal antibodies became rapidly cointernalized (38–40). Recently, serial analysis of gene expression showed CD74 overexpression in pancreatic cancer (16). In the present study, we confirmed that CD74 was positive in 52 cases (78%) and was overexpressed in cancer cells compared with the pancreatic duct in clinical cases. We suggest that CD74 might also be a novel therapeutic target in pancreatic cancer, especially with perineural invasion.

Although the intracellular portion of CD74 seems to lack a signal-transducing domain, cell proliferation and inhibition of apoptosis through extracellular signal-regulated kinase 1/2 are induced by binding of macrophage migration inhibitory factor (41). Secretion of macrophage migration inhibitory factor is seen in both pancreatitis and pancreatic cancer and induces the production or expression of inflammatory molecules, including IFN-γ (42). IFN-γ also induces further expression of cell surface CD74 (43). Hence, CD74 and these associated molecules might play an important role in the perineural invasion of pancreatic cancer in an autocrine/paracrine manner. Moreover, CD74 has a chondroitin sulfate binding site at the extracellular portion, and this can bind cell surface CD44 (44). CD44 is also expressed in pancreatic cancer and human peripheral nerves. Regarding cancer cell-nerve interaction, interaction of CD74 with CD44 may result in cellular activation and migration and promote perineural invasion.

In addition to CD74, some of the up-regulated genes identified in the present analysis have been recently correlated with tumor growth and invasion in pancreatic cancer. For example, tissue plasminogen activator is a serine protease that catalyses the activation of plasminogen. It is required for cell proliferation and angiogenesis in the early stage of pancreatic cancer (45). γ-Synuclein was initially found in infiltrating breast cancer and was referred to as breast carcinoma-specific gene 1. Overexpression of γ-synuclein protein in pancreatic cancer was correlated with perineural invasion and lymph node metastasis in clinical cases (46).

In conclusion, although the precise mechanism remains to be elucidated, overexpression of CD74 was closely associated with perineural invasion in human pancreatic cancer. We think that this perineural invasion model is the first such report and is an appropriate model for analyzing the mechanism of perineural invasion of human pancreatic cancer.

Acknowledgments

We thank H. Suzuki and Y. Nakamura for technical assistance.

References

1. Jemal A, Murray T, Ward E, et al. Cancer statistics, 2005. CA Cancer J Clin 2005;55:10–30.
2. Parkin DM, Bray FI, Devesa SS. Cancer burden in the year 2000. The global picture. Eur J Cancer 2001;37 Suppl 8:S4–66.
3. Sperti C, Pasquali C, Piccoli A, Pedrazzoli S. Recurrence after resection for ductal adenocarcinoma of the pancreas. World J Surg 1997;21:195–200.
4. Hermanek P. Pathology and biology of pancreatic ductal adenocarcinoma. Langenbecks Arch Surg 1998;383:116–20.
5. Gebhardt C, Meyer W, Reichel M, Wunsch PH. Prognostic factors in the operative treatment of ductal pancreatic carcinoma. Langenbecks Arch Surg 2000; 385:14–20.
6. Amikura K, Kobari M, Matsuno S. The time of occurrence of liver metastasis in carcinoma of the pancreas. Int J Pancreatol 1995;17:139–46.

7. Pour PM, Bell RH, Batra SK. Neural invasion in the staging of pancreatic cancer. Pancreas 2003;26: 322–5.
8. Tsiotos GG, Farnell MB, Sarr MG. Are the results of pancreatectomy for pancreatic cancer improving? World J Surg 1999;23:913–9.
9. Sperti C, Pasquali C, Piccoli A, Pedrazzoli S. Survival after resection for ductal adenocarcinoma of the pancreas. Br J Surg 1996;83:625–31.
10. Bardeesy N, DePinho RA. Pancreatic cancer biology and genetics. Nat Rev Cancer 2002;2:897–909.
11. Crnogorac-Jurcevic T, Efthimiou E, Nielsen T, et al. Expression profiling of microdissected pancreatic adenocarcinomas. Oncogene 2002;21:4587–94.
12. Crnogorac-Jurcevic T, Efthimiou E, Capelli P, et al. Gene expression profiles of pancreatic cancer and stromal desmoplasia. Oncogene 2001;20:7437–46.
13. Han H, Bearss DJ, Browne LW, Calaluce R, Nagle RB, Von Hoff DD. Identification of differentially expressed genes in pancreatic cancer cells using cDNA microarray. Cancer Res 2002;62:2890–6.
14. Iacobuzio-Donahue CA, Maitra A, Shen-Ong GL, et al. Discovery of novel tumor markers of pancreatic cancer using global gene expression technology. Am J Pathol 2002;160:1239–49.
15. Iacobuzio-Donahue CA, Ashfaq R, Maitra A, et al. Highly expressed genes in pancreatic ductal adenocarcinomas: a comprehensive characterization and comparison of the transcription profiles obtained from three major technologies. Cancer Res 2003;63: 8614–22.
16. Hustinx SR, Cao D, Maitra A, et al. Differentially expressed genes in pancreatic ductal adenocarcinomas identified through serial analysis of gene expression. Cancer Biol Ther 2004;3:e19–26.
17. Nomura H, Nishimori H, Yasoshima T, et al. A new liver metastatic and peritoneal dissemination model established from the same human pancreatic cancer cell line: analysis using cDNA macroarray. Clin Exp Metastasis 2002;19:391–9.
18. Sclabas GM, Fujioka S, Schmidt C, et al. Overexpression of tropomysin-related kinase B in metastatic human pancreatic cancer cells. Clin Cancer Res 2005; 11:440–9.
19. Chuma M, Sakamoto M, Yasuda J, et al. Overexpression of cortactin is involved in motility and metastasis of hepatocellular carcinoma. J Hepatol 2004;41:629–36.
20. Japan Pancreas Society. Classification of pancreatic cancer. 2nd English ed. Tokyo: Kanehara; 2003.
21. Kameda K, Shimada H, Ishikawa T, et al. Expression of highly polysialylated neural cell adhesion molecule in pancreatic cancer neural invasive lesion. Cancer Lett 1999;137:201–7.
22. Ishikawa O, Ohigashi H, Sasaki Y, et al. Liver perfusion chemotherapy via both the hepatic artery and portal vein to prevent hepatic metastasis after extended pancreatectomy for adenocarcinoma of the pancreas. Am J Surg 1994;168:361–4.
23. Nitecki SS, Sarr MG, Colby TV, van Heerden JA. Long-term survival after resection for ductal adenocarcinoma of the pancreas. Is it really improving? Ann Surg 1995;221:59–66.
24. Takahashi T, Ishikura H, Motohara T, Okushiba S, Dohke M, Katoh H. Perineural invasion by ductal adenocarcinoma of the pancreas. J Surg Oncol 1997;65: 164–70.
25. Miknyoczki SJ, Lang D, Huang L, Klein-Szanto AJ, Dionne CA, Ruggeri BA. Neurotrophins and Trk receptors in human pancreatic ductal adenocarcinoma: expression patterns and effects on *in vitro* invasive behavior. Int J Cancer 1999;81:417–27.
26. Zhu Z, Friess H, di Mola FF, et al. Nerve growth factor expression correlates with perineural invasion and pain in human pancreatic cancer. J Clin Oncol 1999; 17:2419–28.
27. Iwahashi N, Nagasaka T, Tezel G, et al. Expression of glial cell line-derived neurotrophic factor correlates with perineural invasion of bile duct carcinoma. Cancer 2002;94:167–74.
28. Yamaguchi R, Nagino M, Oda K, Kamiya J, Uesaka K, Nimura Y. Perineural invasion has a negative impact on survival of patients with gallbladder carcinoma. Br J Surg 2002;89:1130–6.
29. Ayala GE, Wheeler TM, Shine HD, et al. *In vitro* dorsal root ganglia and human prostate cell line interaction: redefining perineural invasion in prostate cancer. Prostate 2001;49:213–23.
30. Ayala GE, Dai H, Ittmann M, et al. Growth and survival mechanisms associated with perineural invasion in prostate cancer. Cancer Res 2004;64:6082–90.
31. Yonou H, Yokose T, Kamijo T, et al. Establishment of a novel species- and tissue-specific metastasis model of human prostate cancer in humanized non-obese diabetic/severe combined immunodeficient mice engrafted with human adult lung and bone. Cancer Res 2001;61:2177–82.
32. Lock RB, Liem N, Farnsworth ML, et al. The nonobese diabetic/severe combined immunodeficient (NOD/SCID) mouse model of childhood acute lymphoblastic leukemia reveals intrinsic differences in biologic characteristics at diagnosis and relapse. Blood 2002;99:4100–8.
33. Sipos B, Moser S, Kalthoff H, Torok V, Lohr M, Kloppel G. A comprehensive characterization of pancreatic ductal carcinoma cell lines: towards the establishment of an *in vitro* research platform. Virchows Arch 2003;442:444–52.
34. Barrera CA, Almanza RJ, Ogra PL, Reyes VE. The role of the invariant chain in mucosal immunity. Int Arch Allergy Immunol 1998;117:85–93.
35. Hippo Y, Yashiro M, Ishii M, et al. Differential gene expression profiles of scirrhous gastric cancer cells with high metastatic potential to peritoneum or lymph nodes. Cancer Res 2001;61:889–95.
36. Ishigami S, Natsugoe S, Tokuda K, et al. Invariant chain expression in gastric cancer. Cancer Lett 2001; 168:87–91.
37. Jiang Z, Xu M, Savas L, LeClair P, Banner BF. Invariant chain expression in colon neoplasms. Virchows Arch 1999;435:32–6.
38. Burton JD, Ely S, Reddy PK, et al. CD74 is expressed by multiple myeloma and is a promising target for therapy. Clin Cancer Res 2004;10:6606–11.
39. Michel RB, Rosario AV, Andrews PM, Goldenberg DM, Mattes MJ. Therapy of small subcutaneous B-lymphoma xenografts with antibodies conjugated to radionuclides emitting low-energy electrons. Clin Cancer Res 2005;11:777–86.
40. Griffiths GL, Mattes MJ, Stein R, et al. Cure of SCID mice bearing human B-lymphoma xenografts by an anti-CD74 antibody-anthracycline drug conjugate. Clin Cancer Res 2003;9:6567–71.
41. Leng L, Metz CN, Fang Y, et al. MIF signal transduction initiated by binding to CD74. J Exp Med 2003; 197:1467–76.
42. Calandra T, Roger T. Macrophage migration inhibitory factor: a regulator of innate immunity. Nat Rev Immunol 2003;3:791–800.
43. Albanesi C, Cavani A, Girolomoni G. Interferon-gamma-stimulated human keratinocytes express the genes necessary for the production of peptide-loaded MHC class II molecules. J Invest Dermatol 1998;110: 138–42.
44. Naujokas MF, Morin M, Anderson MS, Peterson M, Miller J. The chondroitin sulfate form of invariant chain can enhance stimulation of T cell responses through interaction with CD44. Cell 1993;74:257–68.
45. Diaz VM, Planaguma J, Thomson TM, Reventos J, Paciucci R. Tissue plasminogen activator is required for the growth, invasion, and angiogenesis of pancreatic tumor cells. Gastroenterology 2002;122: 806–19.
46. Li Z, Sclabas GM, Peng B, et al. Overexpression of synuclein-gamma in pancreatic adenocarcinoma. Cancer 2004;101:58–65.

JEM ARTICLE

Essential roles of DC-derived IL-15 as a mediator of inflammatory responses in vivo

Toshiaki Ohteki,[1] Hiroyuki Tada,[1] Kazuto Ishida,[1] Taku Sato,[1] Chikako Maki,[2] Taketo Yamada,[3] Junji Hamuro,[2] and Shigeo Koyasu[2,4]

[1]Department of Immunology, Akita University School of Medicine, Akita 010-8543, Japan
[2]Department of Microbiology and Immunology and [3]Department of Pathology, Keio University School of Medicine, Tokyo 160-8582, Japan
[4]Core Research for Evolutional Science and Technology, Japan Science and Technology Agency, Kawaguchi 332-0012, Japan

Interleukin (IL)-15 is expressed in a variety of inflammatory diseases. However, the contribution of dendritic cell (DC)–derived IL-15 to the development of diseases is uncertain. Using established models of *Propionibacterium acnes* (*P. acnes*)– and zymosan-induced liver inflammation, we observed granuloma formation in the livers of wild-type (WT) and RAG-2$^{-/-}$ mice but not in those of IL-15$^{-/-}$ mice. We demonstrate that this is likely caused by an impaired sequential induction of IL-12, IFN-γ, and chemokines necessary for monocyte migration. Likewise, lethal endotoxin shock was not induced in *P. acnes*– and zymosan-primed IL-15$^{-/-}$ mice or in WT mice treated with a new IL-15–neutralizing antibody. In both systems, proinflammatory cytokine production was impaired. Surprisingly, neither granuloma formation, lethal endotoxin shock, nor IL-15 production was induced in mice deficient for DCs, and adoptive transfer of WT but not IL-15$^{-/-}$ DCs restored the disease development in IL-15$^{-/-}$ mice. Collectively, these data indicate the importance of DC-derived IL-15 as a mediator of inflammatory responses in vivo.

CORRESPONDENCE
Toshiaki Ohteki:
tohteki@med.akita-u.ac.jp

Abbreviations used: BMDC, BM-derived DC; DAB, 3,3′-diaminobenzidine; DTR, diphtheria toxin receptor; DTR tg, CD11c-DTR-GFP transgenic; GOT and GPT, glutamic-oxaloacetic and -pyruvic transaminase, respectively; GSH, glutathione; H&E, hematoxylin and eosin; HRP, horseradish peroxidase; RA, rheumatoid arthritis.

Proper activation followed by inactivation of immune responses is essential for the maintenance of immunological homeostasis in vivo. Prolonged or aberrant activation of immune responses cause a variety of immunopathological disorders, which often result in tissue destruction mediated by effector cells and cytokines.

We and others have found that IL-15 is a pivotal cytokine for the development and function of innate immune cells, including NK cells, NKT cells, TCR-γδ$^+$ intestinal intraepithelial lymphocytes, and DCs (1–9). IL-15 also affects the acquired immune system because the proliferation and survival of CD8$^+$ T cells with naive and memory phenotypes, as well as antigen-specific memory CD8$^+$ T cells, are impaired in both IL-15Rα$^{-/-}$ and IL-15$^{-/-}$ mice (4, 6, 10–12). These studies showed a beneficial effect of IL-15 on the establishment and maintenance of the immune system against pathogen infections as well as malignancies.

In contrast, circumstantial evidence suggests that IL-15 is also involved in the development of immunopathological disorders. IL-15 mRNA and protein are expressed in synovial membranes in rheumatoid arthritis (RA) (13, 14). It has been suggested that IL-15 precedes TNF-α production in cytokine cascade to recruit T cells into the synovial membranes, possibly contributing to the pathogenesis of RA (13, 14). Supporting this notion, treatment of DBA/1 mice with the soluble IL-15Rα and IL-15 mutant/Fcγ2a fusion protein, which bind the IL-15R with high affinity but do not trigger signaling events, prevents the mice from developing collagen-induced arthritis (15, 16). The elevated numbers of IL-15–expressing cells and/or elevated levels of IL-15 production correlate with the activities of inflammatory bowel disease (17), type C chronic liver disease (18), sarcoidosis (19), and multiple sclerosis (20). These observations suggest a harmful effect of IL-15 in various immunopathological and inflammatory diseases. However, as IL-15 is produced by many cell types, it remains unknown whether development of these diseases attributes to DC-derived IL-15.

In this study we generated new mAbs to detect and block mouse IL-15 activity and established an ELISA system that enabled us to examine the amounts of IL-15 at protein

T. Ohteki and H. Tada contributed equally to this work.
The online version of this article contains supplemental material.

level. Using the mAb and ELISA system combined with gene-targeted mice, we investigated the role of IL-15 in well-characterized inflammatory disease models in mice. We demonstrate that IL-15 is essential for *P. acnes*– and zymosan-induced granuloma formation and subsequent LPS-induced endotoxin shock, as well as liver damage, through induction of proinflammatory cytokines and chemokines. Of interest, the development of liver diseases and endotoxin shock is unaffected in the absence of T, B, and NK cells, whereas it was severely affected in mice lacking DC-derived IL-15. These experiments identify an irreplaceable function of DC-derived IL-15 in bacterial product–mediated inflammatory responses.

RESULTS

Impaired granuloma formation in IL-15$^{-/-}$ mice

P. acnes is suspected to be a causative bacteria for human sarcoidosis, and its cell wall components show strong immunoadjuvant activities, which induce monocyte migration into the liver and granuloma formation (21–23).

To examine the role of IL-15 in the granuloma formation in vivo, control WT and IL-15$^{-/-}$ mice were injected with heat-killed *P. acnes*. Consistent with previous reports (21–23), granuloma formation was evident in the liver of WT mice on day 6 after injection, whereas it was hardly seen in that of IL-15$^{-/-}$ mice (Fig. 1 A, top left and top middle). Importantly, the granuloma formation was substantially restored by IL-15 injection into IL-15$^{-/-}$ mice (Fig. 1 A, top right). It has been reported that on *P. acnes* infection circulating DC precursors migrate into the liver and, in cooperation with Kupffer cells, monocytes, and T cells, participate in the granulomatous reaction (24). Indeed, *P. acnes*–induced granulomas contained CD11c^{+} DCs (Fig. 1 B). The granuloma formation was observed in the liver of RAG-2$^{-/-}$ mice and NK cell–depleted RAG-2$^{-/-}$ mice but was absent in that of IL-15$^{-/-}$RAG-2$^{-/-}$ mice (Fig. 1 A, bottom; and Fig. S1, available at

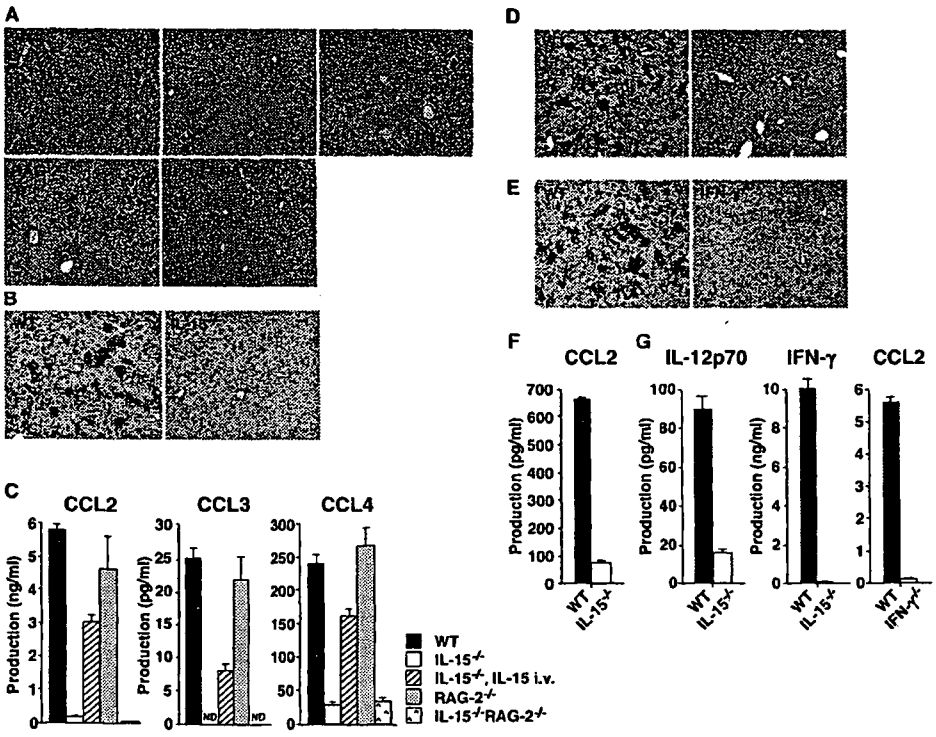

Figure 1. IL-15$^{-/-}$ mice fail to develop *P. acnes*– and zymosan-induced granulomas. (A) Granuloma formation in the liver of WT, IL-15$^{-/-}$, RAG-2$^{-/-}$, and IL-15$^{-/-}$RAG-2$^{-/-}$ mice. Livers were taken on day 6 after a 0.5-mg heat-killed *P. acnes* injection, and sections were stained with H&E. Bar, 100 μm. (B) The liver sections of *P. acnes*–injected WT and IL-15$^{-/-}$ mice were stained with biotinylated anti-CD11c mAb and streptavidin-HRP and further visualized with DAB. Slides were counterstained with Mayer's hematoxylin. Bar, 100 μm. (C) Chemokine levels in the sera of WT, IL-15$^{-/-}$, RAG-2$^{-/-}$, and IL-15$^{-/-}$RAG-2$^{-/-}$ mice were assessed by ELISA at 72 h after a 0.5-mg heat-killed *P. acnes* injection. Values represent SD (n = 3 mice/group). Data are representative of two to four experiments. (D) Granuloma formation in the liver of zymosan-injected WT and IL-15$^{-/-}$ mice. Livers were taken on day 6 after a 1 mg zymosan injection, and sections were stained with biotinylated anti-CD11c mAb and streptavidin-HRP and further visualized with DAB. Slides were counterstained with Mayer's hematoxylin. Bar, 100 μm. (E) The liver sections of *P. acnes*–injected WT and IFN-γ$^{-/-}$ mice were stained as described in B. Bar, 100 μm. (F) 3 d after a 1-mg zymosan injection, CCL2 in the sera of WT and IL-15$^{-/-}$ mice was measured by ELISA. Data are representative of four experiments. (G) 3 d after a 0.5-mg *P. acnes* injection, IL-12p70, and IFN-γ in the sera of WT and IL-15$^{-/-}$ mice and CCL2 in the sera of WT and IFN-γ$^{-/-}$ mice were measured by ELISA. Values represent SD (n = 3 mice/group). Data are representative of three experiments.

http://www.jem.org/cgi/content/full/jem.20061297/DC1), indicating that both T, B, and NK cells are dispensable in the process of granuloma formation. Because chemokine production is critical for monocyte migration into the liver, we next examined the chemokine production, in particular MCP-1 (CCL2) and MIP-1α/β (CCL3/4), which are critical chemoattractants for monocytes. On day 3 after *P. acnes* injection, considerable levels of these chemokines were detected in the sera of WT, RAG-$2^{-/-}$, and NK cell–depleted RAG-$2^{-/-}$ mice (Fig. 1 C and Fig. S2, available at http://www.jem.org/cgi/content/full/jem.20061297/DC1). In contrast, these chemokines were produced only marginally in IL-$15^{-/-}$ and IL-$15^{-/-}$RAG-$2^{-/-}$ mice (Fig. 1 C). Again, the chemokine production was restored by IL-15 injection into IL-$15^{-/-}$ mice. To further examine whether IL-15 directly controls the chemokine production, we analyzed IFN-$\gamma^{-/-}$ mice. As reported previously (23), *P. acnes*–induced granuloma formation was not seen in the liver of IFN-$\gamma^{-/-}$ mice (Fig. 1 E). In addition, we found that *P. acnes*–induced IL-12p70 and IFN-γ production in IL-$15^{-/-}$ and CCL2 production in IFN-$\gamma^{-/-}$ mice was impaired (Fig. 1 G), indicating that IL-15 indirectly induces chemokine production by regulating the IL-12–IFN-γ axis in vivo.

Zymosan is a yeast cell wall particle containing β-glucan and mannan as major components. As *P. acnes* does, zymosan can activate and recruit monocytes, macrophages, and leukocytes (25–27), resulting in the secretion of inflammatory cytokines, hydrogen peroxide, and arachidonic acid (28–30). We also used zymosan to examine the role for IL-15 in the granuloma formation. Consistent with previous experiments (31), zymosan recruited monocytes and DCs and induced granuloma formation in the liver of WT mice. Again, the granulomas were not seen in the liver of IL-$15^{-/-}$ mice (Fig. 1 D), likely because of the lack of chemokine production, such as CCL2 (Fig. 1 F) (31). Our results collectively indicate that IL-15 controls *P. acnes*– and zymosan-induced granuloma formation, likely through the regulation of chemokine production in vivo.

IL-15 regulates LPS-induced lethal endotoxin shock

LPS injection into *P. acnes*–primed mice stimulates DCs and macrophages to produce large amounts of proinflammatory cytokines such as IL-12, IFN-γ, and TNF-α, which cause lethal endotoxin shock in vivo (32–34). Likewise, LPS injection into zymosan-primed mice induces shock and tissue injury (35). We next examined the role of IL-15 in LPS-induced endotoxin shock. On day 6 after a 0.5-mg heat-killed *P. acnes* injection, 1 μg LPS was injected into WT and IL-$15^{-/-}$ mice to induce lethal endotoxin shock. As reported (32–34), *P. acnes*–primed WT mice were sensitive to LPS-induced endotoxin shock, and all mice died within a day. In contrast, IL-$15^{-/-}$ mice were strongly resistant and survived (Fig. 2 A). In addition, NK cell–depleted WT mice, RAG-$2^{-/-}$, mice and NK cell–depleted RAG-$2^{-/-}$ mice died just as control WT mice did, indicating that proinflammatory cytokines produced by T, B, and NK cells are dispensable for the endotoxin shock induction (Fig. 2 A).

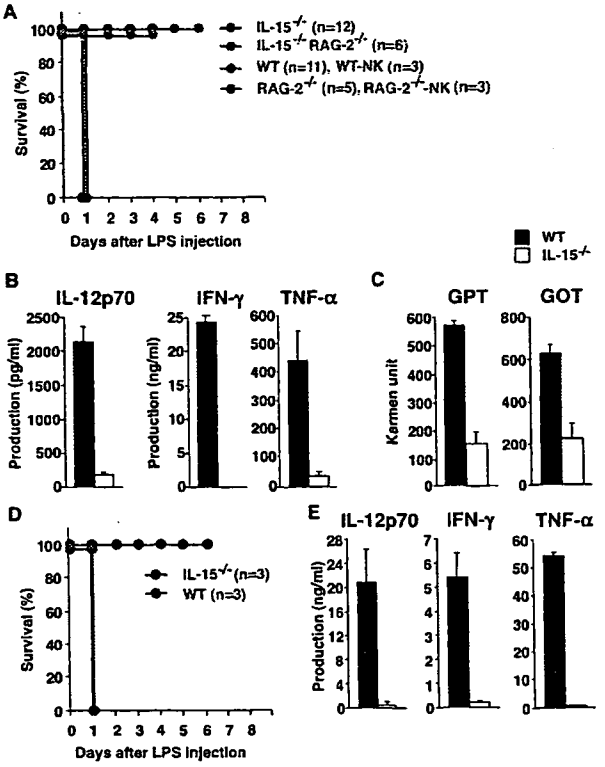

Figure 2. IL-$15^{-/-}$ mice are resistant to LPS-induced lethal endotoxin shock. (A) On day 6 after a 0.5-mg heat-killed *P. acnes* injection, 1 μg LPS were further injected into the indicated mice to induce lethal endotoxin shock. To deplete NK cells, mice were intraperitoneally injected with 300 μg of anti-asialo GM1 polyclonal antibody on the day before and day 3 after *P. acnes* injection. (B) Serum levels of IL-12p70, IFN-γ, and TNF-α were measured by ELISA in *P. acnes*–primed mice at 2 h after LPS injection. Values represent SD (n = 3 WT and 2 IL-$15^{-/-}$ mice/group). Data are representative of three experiments. (C) Serum GOT and GPT levels were assessed in *P. acnes*–primed mice at 2 h after LPS injection. Values represent SD (n = 3 mice/group). Data are representative of two to four experiments. (D) On day 6 after a 1-mg zymosan injection, 10 μg LPS was injected into the indicated mice, and the survival of the mice was monitored. (E) Serum levels of IL-12p70, IFN-γ, and TNF-α were measured by ELISA in zymosan-primed mice at 2 h after LPS injection. Values represent SD (n = 3 mice/group). Data are representative of three experiments.

IL-12, IFN-γ, and TNF-α are known to play important roles in induction of liver injury and/or endotoxin shock (23, 34, 36–39). We thus examined the production of proinflammatory cytokines, in particular IL-12p70, IFN-γ, and TNF-α, in control WT and IL-$15^{-/-}$ mice (Fig. 2 B). Shortly after LPS injection (2 h), these cytokines were detected in the sera of control WT mice, whereas only small amounts of these cytokines were produced in the sera of IL-$15^{-/-}$ mice (Fig. 2 B). Because these cytokines cause liver injury, the level of serum glutamic-pyruvic transaminase (GPT) and glutamic-oxaloacetic transaminase (GOT), an index for hepatocyte damage, was also measured. As expected from the

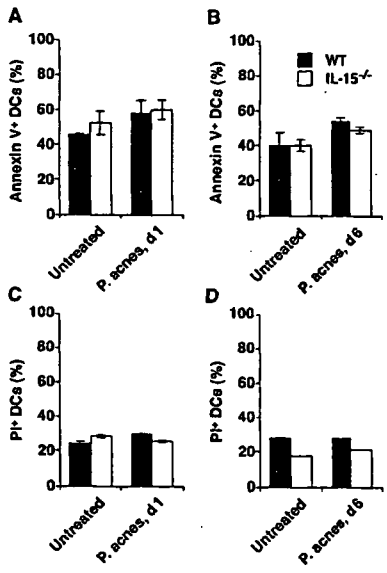

Figure 3. Unaffected apoptosis in IL-15$^{-/-}$ DCs. Splenic DCs were obtained from NK cell-depleted WT and IL-15$^{-/-}$ mice before (untreated) and 1 d (*P. acnes*, d1) and 6 d (*P. acnes*, d6) after heat-killed *P. acnes* injection. (A and B) The proportions of annexin V$^+$ DCs of WT and IL-15$^{-/-}$ mice are shown. (C and D) The proportions of propidium iodide–positive DCs of WT and IL-15$^{-/-}$ mice are shown. Values represent SD (n = 2 mice/group). Data are representative of three experiments.

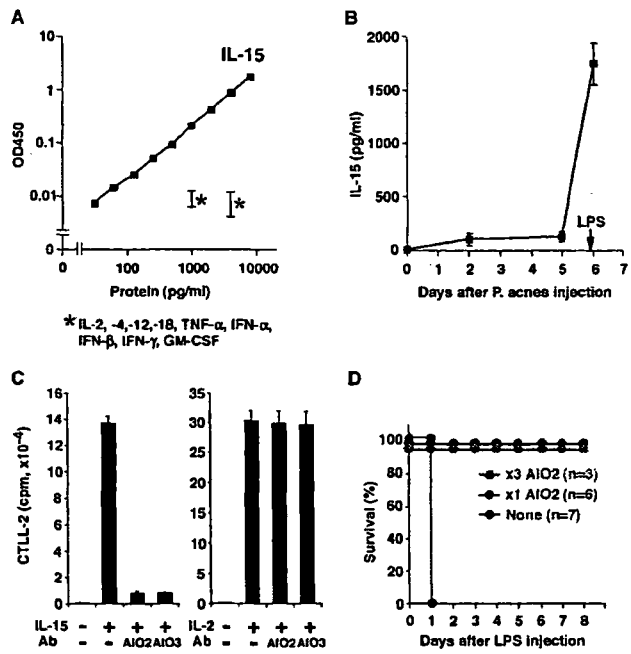

Figure 4. Quantification of IL-15 protein levels by ELISA and treatment of endotoxin shock by IL-15 neutralizing antibody. (A) Newly generated ELISA was specific for mouse IL-15. Specificity of one anti–IL-15 mAb (AIO3) was tested by using the panel of cytokines indicated in the figure. (B) Detection of IL-15 protein in the sera of *P. acnes*– and LPS-injected WT mice. Serum samples were collected from WT and IL-15$^{-/-}$ mice on days 2 and 5 after *P. acnes* injection and at 1.5 h after a subsequent LPS injection on day 6, and levels of IL-15 were assessed with our IL-15 ELISA system. Values represent SD (n = 3 mice/group). Data are representative of two to four experiments. (C) To test the capacity of AIO2 and AIO3 to block IL-15 activities, 5 × 10^4 CTLL-2 cells were stimulated with 10 ng/ml IL-15 or IL-2 in the presence or absence of 10 μg/ml AIO2 or AIO3 for 24 h and pulsed with [^{3}H]thymidine for an additional 8 h. Values represent SD of triplicate cultures. Data are representative of two to four experiments. (D) To examine whether AIO2 can block IL-15 activities in vivo, WT mice were injected with 0.5 mg AIO2 either on day 0, 3, or 6 (x3 AIO2) or only on day 6 (x1 AIO2) after *P. acnes* injection. On day 6, 1 h after AIO2 injection, 1 μg LPS was further injected, and survival of these mice was monitored.

minimal proinflammatory cytokine production, considerable reduction of GPT and GOT release was observed in the sera of IL-15$^{-/-}$ mice, as compared with those in WT mice (Fig. 2 C). Similar to these observations, zymosan-primed IL-15$^{-/-}$ mice exhibited strong resistance to LPS-induced lethality, which was consistent with the reduced production of IL-12, IFN-γ, and TNF-α (Fig. 2, D and E).

Unaffected DC survival in IL-15$^{-/-}$ mice

As recently reported that IL-15 regulates survival of DCs (40), impaired inflammatory responses observed in IL-15$^{-/-}$ mice might be caused by the impaired DC survival. To examine this possibility, we examined the number of splenic DCs between WT and IL-15$^{-/-}$ mice before and after *P. acnes* injection. The numbers of DCs in untreated WT and IL-15$^{-/-}$ mice were 0.83 × 10^6 ± 0.15 (n = 5) and 0.82 × 10^6 ± 0.13 (n = 5), respectively, and those in *P. acnes*–injected WT and IL-15$^{-/-}$ mice (6 d after injection) were 1.39 × 10^6 ± 0.28 (n = 4) and 1.54 × 10^6 ± 0.16 (n = 4), respectively. Using annexin V and propidium iodide staining, we further analyzed the number of apoptotic DCs before and after *P. acnes* injection and found no important difference between WT and IL-15$^{-/-}$ DCs (Fig. 3). These results suggested that impaired inflammatory responses observed in IL-15$^{-/-}$ mice are unlikely caused by the impaired DC survival in vivo.

mAb generation to detect and block mouse IL-15 activity

As IL-15 was found to be a critical mediator for granuloma formation and endotoxin shock induction in vivo, it is important to quantitate the amount of IL-15 produced as a soluble protein in mice during the induction phase of granuloma formation and the eliciting phase of endotoxin shock. For this purpose, we generated rat mAbs specific for mouse IL-15 (for details see Materials and methods). Among 108 clones, 2 clones named AIO2 and AIO3 produced mAbs against mouse IL-15, which were suitable as coating antibodies for an ELISA system. Importantly, the newly developed ELISA system is specific for mouse IL-15 and does not cross react with other cytokines tested, which include IL-2, IL-4, IL-12, TNF-α, IFN-α, IFN-β, IFN-γ, and GM-CSF (Fig. 4 A). Using the ELISA system, we found that substantial amounts of IL-15 were produced in the sera of *P. acnes*–injected WT mice, and the IL-15 levels were dramatically enhanced immediately after LPS injection into *P. acnes*–primed WT mice (Fig. 4 B),

which was consistent with the observation that the lack of IL-15 resulted in the impaired endotoxin shock.

The results shown in Fig. 2 (A and D) and Fig. 4 B collectively raised a possibility of treatment of inflammatory diseases by blocking IL-15 activity in vivo. To this end, we examined whether anti–IL-15 mAbs were capable of blocking IL-15 activity (Fig. 4 C). It is well known that both IL-2 and IL-15 efficiently induce proliferation of a T cell line, CTLL-2. As shown in Fig. 4 C, IL-15–dependent proliferation of CTLL-2 was markedly reduced (>95% reduction) in the presence of AIO2 or AIO3, whereas IL-2–dependent proliferation of CTLL-2 was not affected at all by these mAbs, demonstrating that the mAbs efficiently and selectively block IL-15 activity in vitro. We further examined the effect of AIO2 in vivo (Fig. 4 D). WT mice that had been injected with AIO2 on days 0, 3, and 6 after *P. acnes* injection (x3 AIO2) and only on day 6 (1 h before LPS injection, x1 AIO2) were strongly resistant to LPS-induced lethality and survived. The results

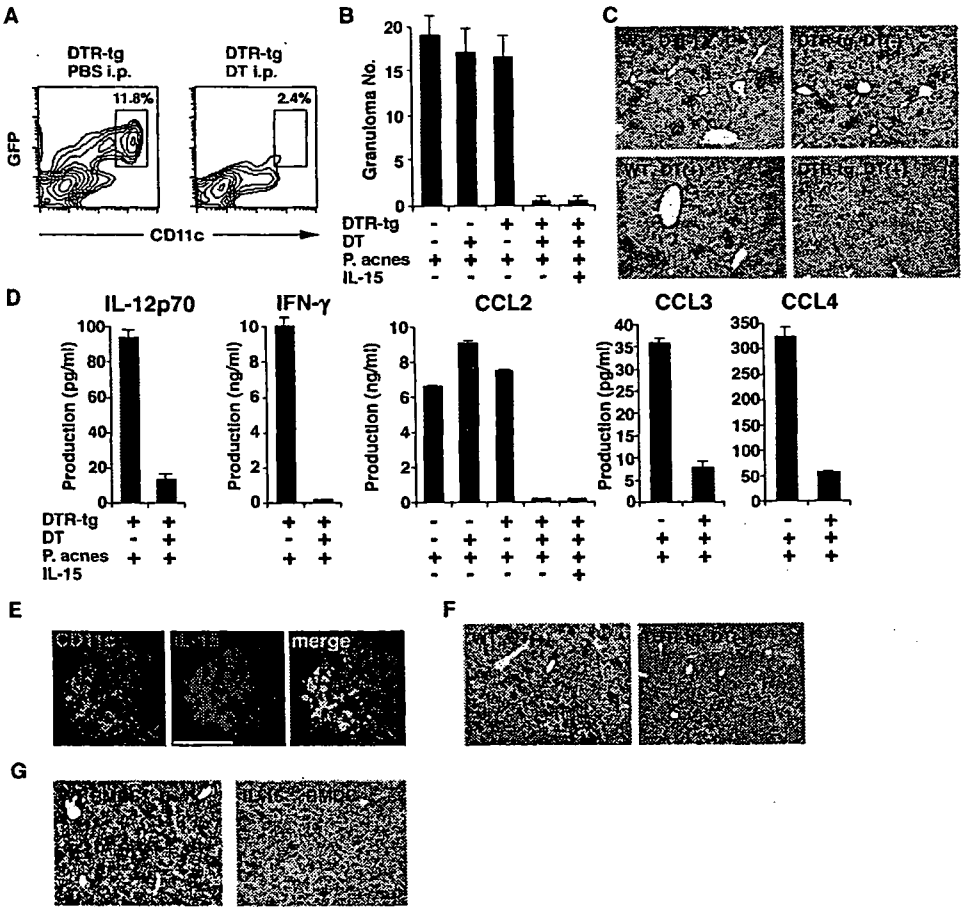

Figure 5. DC-derived IL-15 controls granuloma formation. (A) Spleen cells were obtained from DTR tg mice 24 h after injection of 100 ng DT or PBS and stained with anti-CD11c-PE. The percentages indicate the proportions of DCs in a DC-enriched fraction; i.e., the cells at the interface after a dense BSA gradient centrifugation (see DC preparation... in Materials and methods). (B) Granuloma formation in the liver of *P. acnes*-primed DT-injected DTR tg mice. On day 3 after a 0.5-mg heat-killed *P. acnes* injection, livers were taken from WT and DTR tg mice that had been injected with either PBS or DT on the day before *P. acnes* injection, and sections were stained with H&E. Numbers of granulomas were counted in five different fields under a microscope. Values represent SD (n = 3 mice/group). Data are representative of three experiments. (C) To test whether DCs were present in the granuloma regions, the liver sections were stained with biotinylated anti-CD11c mAb and streptavidin-HRP and further visualized with DAB. Slides were counterstained with Mayer's hematoxylin. Bar, 100 μm. (D) IL-12p70, IFN-γ, and chemokine levels in the sera of DT-injected DTR tg mice were assessed by ELISA at 72 h after a 0.5-mg heat-killed *P. acnes* injection. Values represent SD (n = 3 mice/group). Data are representative of three experiments. (E) Immunofluoresence staining for the identification of IL-15–producing cells. Acetone-fixed frozen tissue sections were incubated with FITC-conjugated anti-CD11c (clone N418) and biotinylated anti–IL-15 antibodies and further developed with streptavidin-PE. Bar, 50 μm. (F) Granuloma formation in the liver of zymosan-primed DT-injected DTR tg mice. As described in B and C, livers were taken from the indicated mice on day 3 after a 1-mg zymosan injection, and sections were stained for CD11c. Slides were counterstained with Mayer's hematoxylin. Bar, 100 μm. (G) Granuloma formation in the liver of BMDC-injected IL-15$^{-/-}$ mice. IL-15$^{-/-}$ mice were injected with 1 × 10^6 WT BMDCs or IL-15$^{-/-}$ BMDCs. After 12 h, mice were injected with 0.5 mg *P. acnes*, and granuloma formation was analyzed 6 d later as described in B, C, and F. Bar, 100 μm.

clearly show that antibody capable of neutralizing IL-15 activity is effective in blocking endotoxin shock in vivo.

Essential roles for DC-derived IL-15 in inflammatory response induction

As DCs are present in granuloma regions (Fig. 1, B, D, and E), we further examined the role of DCs in the granuloma formation using CD11c–diphtheria toxin receptor (DTR)–GFP transgenic (DTR tg) mice (41). Because the mice carry a transgene encoding DTR-GFP fusion protein under the control of a mouse CD11c promoter, DT injection induces selective depletion of DCs in vivo (Fig. 5 A) (41). *P. acnes*– and zymosan-induced (Fig. 5, B and C; and Fig. 5 F, respectively) granulomas were observed in the livers of untreated WT, DT-injected WT, and untreated DTR tg mice, as expected. In contrast, neither $CD11c^+$ DCs nor granulomas themselves were observed in the DT-injected DTR tg mice (Fig. 5, B, C, and F). Consistent with this observation, production of IL-12p70, IFN-γ, CCL2, and CCL3/4 was impaired in the DT-injected DTR tg mice, as observed in $IL\text{-}15^{-/-}$ mice (Fig. 5 D). Importantly, immunohistochemical analysis revealed that many IL-15–producing cells in granuloma regions were $CD11c^+$ DCs (Fig. 5 E). Contrary to the case of $IL\text{-}15^{-/-}$ mice, however, IL-15 administration restored neither the *P. acnes*–induced granulomatous liver disease nor CCL2 production in DC-depleted DTR tg mice (Fig. 5, B and D), implying that direct action of DC-derived IL-15 on DCs is necessary for the chemokine-mediated granuloma formation in vivo. To formally demonstrate the importance of DC-derived IL-15 in the granuloma formation, BM-derived DCs (BMDCs) of WT and $IL\text{-}15^{-/-}$ mice were adoptively transferred into $IL\text{-}15^{-/-}$ mice. Importantly, the granuloma formation was substantially restored by the injection of WT but not $IL\text{-}15^{-/-}$ BMDCs into $IL\text{-}15^{-/-}$ mice (Fig. 5 G), demonstrating that DC-derived IL-15 is essential for the granuloma formation.

Intracellular redox status affects the pattern of cytokine production by DCs and macrophages (42–45). For example, reductive DCs (and macrophages) with elevated intracellular glutathione (GSH) preferentially produce IL-12 and are involved in Th1 responses, whereas oxidative DCs with reduced GSH produce IL-10 and PGE_2, which lead to Th2 cell induction. As *P. acnes* priming efficiently induces reductive status in DCs (44), we next examined the role for IL-15 in determining redox status in DCs (Fig. S3, available at http://jem.org.cgi/content/full/jem.20061297/DC1). As previously shown (44), *P. acnes* injection clearly induced a reductive condition with elevated intracellular GSH levels in WT DCs. In contrast, such a reductive condition was not induced, if any, in $IL\text{-}15^{-/-}$ DCs on *P. acnes* stimulation. These data indicate that IL-15 is one of the critical cytokines in reductive DC differentiation.

We also examined the role of DCs in endotoxin shock. 1 d after DT injection, control WT and DTR tg mice were primed with 0.5 mg *P. acnes*. On day 3 after *P. acnes* injection, these mice were injected with 1 μg LPS, and survival rate was monitored. On LPS injection, all *P. acnes*–primed WT and DT-untreated DTR tg mice died of endotoxin shock within 24 h (Fig. 6 A). However, *P. acnes*–primed and DT-injected DTR tg mice survived much longer than control mice, indicating that DCs play a pivotal role in endotoxin shock as well. Of note, DT-injected DTR tg mice survived relatively shorter than $IL\text{-}15^{-/-}$ mice (Fig. 2 A), which was likely because of the gradual recovery of DCs in DT-injected DTR tg mice as reported previously (41). *P. acnes*–primed DT-injected DTR tg mice showed impaired production of IL-15 and IL-15–regulated proinflammatory cytokines, IL-12p70, IFN-γ, and TNF-α on LPS stimulation (Fig. 6 B). In addition, WT BMDC-transferred $IL\text{-}15^{-/-}$ mice became sensitive to the endotoxin shock, and all mice died within a day, whereas $IL\text{-}15^{-/-}$ BMDC–injected $IL\text{-}15^{-/-}$ mice remained resistant (Fig. 6 C). Collectively, these results indicate that DC-derived IL-15 is critical for endotoxin shock induction in vivo.

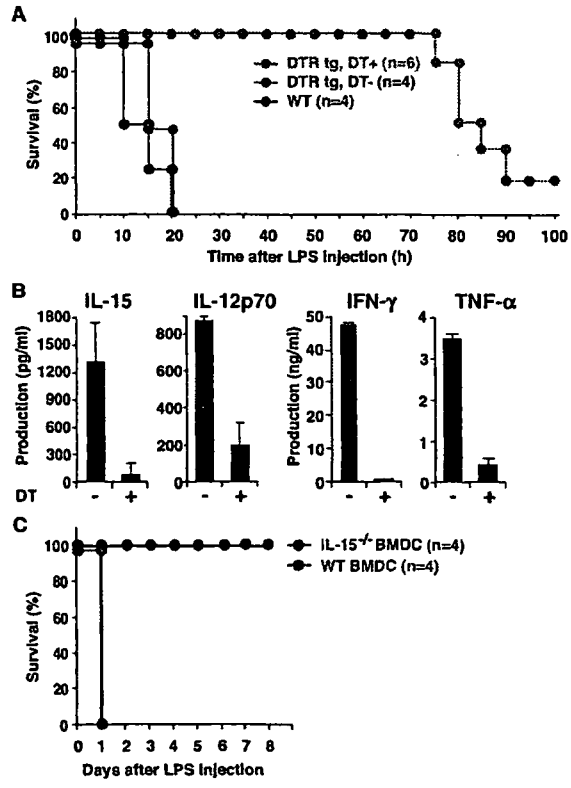

Figure 6. DC-derived IL-15 regulates endotoxin shock. (A) 1 d after DT injection, control WT and DTR tg mice were primed with 0.5 mg *P. acnes*. On day 3 after *P. acnes* injection, these mice were further injected with 1 μg LPS, and survival rate was monitored. (B) Serum levels of IL-15, IL-12p70, IFN-γ, and TNF-α were assessed in DT-injected and *P. acnes*–primed DTR tg mice at 2 h after LPS injection. Values represent SD (n = 3 mice/group). Data are representative of three experiments. (C) $IL\text{-}15^{-/-}$ mice were injected with 1×10^6 WT or $IL\text{-}15^{-/-}$ BMDCs. After 12 h, mice were injected with 0.5 mg *P. acnes*. On day 6 after *P. acnes* injection, these mice were further injected with 5 μg LPS, and survival rate was monitored.

DISCUSSION

DC-derived IL-15

Prolonged or aberrant activation of immune responses cause a variety of immunopathological disorders that are often mediated by effector cells and cytokines. We previously found that DC-derived IL-15 is required for the functional maturation of DCs, such as IL-12 production in response to LPS and agonistic anti-CD40 mAb combined with IL-4 stimulation in vitro (8), and have recently shown that DC-derived IL-15 is essential for CpG-induced protective immune activation against pathogen infections in vivo (9). In contrast to the beneficial effect of DC-derived IL-15, we maintain in this study that DC-derived IL-15 has harmful aspects and causes inflammatory diseases, such as granuloma formation and endotoxin shock in vivo.

IL-15 is involved in a variety of inflammatory and autoimmune diseases (13, 14, 17-20). To address whether development of these diseases attributes to IL-15, analyses using IL-15$^{-/-}$ mice, anti–IL-15 neutralizing antibody, soluble IL-15Rα, and IL-15 mutant/Fcγ2a fusion protein are in progress in both human and mouse models (15, 16). As IL-15 is produced by multiple cell types, which include DCs, macrophages, monocytes, and endothelial cells (5), an advanced and unresolved question has been whether DC-derived IL-15 is exclusively required for the development of certain diseases in vivo. Numerous previous in vitro studies indicated that DC-derived IL-15 is capable of inducing activation of Th1 cells, CTL, NK cells, monocyte differentiation into DCs, and antigen-processing machinery in DCs (5, 46), but these studies did not directly prove the irreplaceable role of DC-derived IL-15 in disease development in vivo, where multiple IL-15 producers are present. To address this issue, it is important to show that the development of certain diseases is impaired in IL-15$^{-/-}$ or WT mice treated with reagents to block IL-15 activity, and to further restore the disease development by adoptively transferring WT but not IL-15$^{-/-}$ DCs into these mice. In this respect, only one paper has shown that IL-15$^{-/-}$ or WT mice treated with soluble IL-15Rα were impaired in CD8$^+$ T cell–dependent delayed-type hypersensitivity response, and the delayed-type hypersensitivity response was restored by injecting antigen-labeled WT DCs in vivo (47). It is unclear, however, whether IL-15 is important for cytokine production or antigen presentation in this study (47). Other groups have shown that IL-15Rα and IL-15 expression by hematopoietic cells is critical for the maintenance of antigen-specific memory CD8$^+$ T cells and bystander CD8$^+$ T cell proliferation through a "transpresentation" pathway (48–53), and implied DCs as the major source of IL-15 but never proved it. Accordingly, it remains unknown whether DC-derived IL-15 is essential in the maintenance of innate and acquired immune responses, and whether it causes inflammatory disease development in vivo. It is thus important to prove the in vivo role of DC-derived IL-15 for the development of antiinflammatory drugs that selectively block the DC-derived IL-15 activity.

Mechanisms of how IL-15 controls cytokine production are unknown. As shown in this paper, IL-15 increased the intracellular GSH levels in DCs. Intracellular GSH levels in DCs and macrophages play an important role in determining the profiles of proinflammatory cytokines (42–45). We have previously demonstrated that reductive DCs with high intracellular GSH levels preferentially produce IFN-γ, which in turn augment GSH levels in the cells (44). As shown in this paper, IL-15 is also one of the positive regulators of intracellular GSH status in DCs, augmenting the production of proinflammatory cytokines. In future studies, it should be determined how IL-15 controls the amounts of intracellular GSH in DCs.

Granuloma formation, liver injury, and IL-15

The number of *P. acnes*–induced granulomas and LPS-induced hepatic necrosis after priming with *P. acnes* are substantially reduced in IFN-γ$^{-/-}$ mice (Fig. 1 E) (23). In addition, *P. acnes* does not induce granuloma formation in TNF-RI$^{-/-}$ mice and mice treated with soluble TNF-RI (21). These studies clearly demonstrate the importance of IFN-γ and TNF-α in *P. acnes*–induced liver diseases in vivo. In contrast, it has been shown that CCL3 attracts DC precursors in the blood into the sinusoidal granuloma and lets them participate in inflammatory responses in *P. acnes*–primed mice (24). In addition, CCL2 has also been reported as an important monocyte chemoattractant for granuloma models induced by zymosan, *P. acnes*, and *Mycobacterium tuberculosis* (54–56). These studies show that the chemokines play a critical role in granuloma models, though the importance of IFN-γ and TNF-α in chemokine production remains unclear. Notably, we determined that an IL-15–IL-12–IFN-γ–chemokine (CCL2/3/4) axis in innate immune system is essential, whereas T and B cells are dispensable for the development of granulomatous disease and/or liver injury. Immunohistochemical analysis revealed that DCs preferentially expressed IL-15 in the granuloma regions, and the granuloma formation was impaired in mice lacking DC and DC-derived IL-15 production, clearly demonstrating that DC-derived IL-15 is an initiator for the development of liver diseases.

Of note, IL-15 injection restored the granuloma formation in the liver of IL-15$^{-/-}$ mice but not DC-depleted DTR tg mice. These results suggest that a critical first step for the granuloma formation is to stimulate DCs with DC-derived IL-15 in an autocrine manner. Although Kupffer cells are critically involved as initial antigen-presenting (*P. acnes* and zymosan) cells (24), Kupffer cells isolated from *P. acnes*–primed mice were unable to produce IL-15 on LPS stimulation in vitro (unpublished data).

Endotoxin shock and IL-15

LPS-induced liver injury is closely coupled to endotoxin shock. Indeed, mice deficient in IL-12, IFN-γ, TNF-α, or the receptors for these cytokines displayed resistance to LPS-induced endotoxin shock (34, 36, 38, 57). We showed in this paper that DCs are essential for endotoxin shock, and